







The neuropeptide pigment-dispersing factor signals independently of Bruchpilot-labelled active zones in daily remodelled terminals of *Drosophila* clock neurons

Benedikt Hofbauer¹ | Meet Zandawala^{1,5}  | Nils Reinhard¹  |
Dirk Rieger¹  | Christian Werner²  | Jan Felix Evers^{3,4}  |
Christian Wegener¹ 

¹Biocenter, Theodor-Boveri-Institute, Neurobiology and Genetics, Julius-Maximilians-Universität Würzburg, Würzburg, Germany

²Biocenter, Theodor-Boveri-Institute, Department of Biotechnology and Biophysics, Julius-Maximilians-Universität Würzburg, Würzburg, Germany

³Centre for organismal studies COS, Universität Heidelberg, Heidelberg, Germany

⁴Cairn GmbH, Heidelberg, Germany

⁵Department of Biochemistry and Molecular Biology, University of Nevada Reno, Reno, NV, USA

Correspondence

Jan-Felix Evers, Cairn GmbH,
Heidebuckelweg 5, 69118 Heidelberg,
Germany.

Email: jfevers@cairn-research.eu

Christian Wegener, Biocenter, Theodor-
Boveri-Institute, Neurobiology and
Genetics, Julius-Maximilians-Universität
Würzburg, Am Hubland, 97074
Würzburg, Germany.

Email: christian.wegener@biozentrum.uni-wuerzburg.de

Funding information

Deutsche Forschungsgemeinschaft,
Grant/Award Number: 251610680, INST
93/809-1 FUGG

Edited by: Giovanni Galizia

Abstract

The small ventrolateral neurons (sLNvs) are key components of the central clock in the *Drosophila* brain. They signal via the neuropeptide pigment-dispersing factor (PDF) to align the molecular clockwork of different central clock neurons and to modulate downstream circuits. The dorsal terminals of the sLNvs undergo daily morphological changes that affect presynaptic sites organised by the active zone protein Bruchpilot (BRP), a homolog of mammalian ELKS proteins. However, the role of these presynaptic sites for PDF release is ill-defined.

Here, we combined expansion microscopy with labelling of active zones by endogenously tagged BRP to examine the spatial correlation between PDF-containing dense-core vesicles and BRP-labelled active zones. We found that the number of BRP-labelled puncta in the sLNv terminals was similar while their density differed between Zeitgeber time (ZT) 2 and 14. The relative distance between BRP- and PDF-labelled puncta was increased in the morning, around the reported time of PDF release. Spontaneous dense-core vesicle release profiles of sLNvs in a publicly available ssTEM dataset (FAFB) consistently lacked spatial correlation to BRP-organised active zones. RNAi-mediated downregulation of *brp* and other active zone proteins expressed by

Abbreviations: AstC, Allatostatin C; BRP, Bruchpilot; CT, circadian time; DD, constant conditions: constant temperature, constant darkness; ExM, expansion microscopy; FAFB, full adult female fly brain; ICC, immunocytochemistry; LD, 12 h light:12 h dark; LL, continuous light; ILNv, large ventrolateral neuron; LNv, ventrolateral neuron; NGS, normal goat serum; PBS, phosphate-buffered saline; PDF, pigment-dispersing factor; ROI, region of interest; sLNv, small ventrolateral neuron; sNPF, short neuropeptide F; ZT, Zeitgeber time.

This is an open access article under the terms of the [Creative Commons Attribution](https://creativecommons.org/licenses/by/4.0/) License, which permits use, distribution and reproduction in any medium, provided the original work is properly cited.

© 2024 The Authors. *European Journal of Neuroscience* published by Federation of European Neuroscience Societies and John Wiley & Sons Ltd.

the sLNvs did not affect PDF-dependent locomotor rhythmicity. In contrast, down-regulation of genes encoding proteins of the canonical vesicle release machinery, the dense-core vesicle-related protein CADPS, as well as PDF impaired locomotor rhythmicity.

Taken together, our study suggests that PDF release from the sLNvs is independent of BRP-organised active zones, while BRP may be redistributed to active zones in a time-dependent manner.

KEYWORDS

ELKS/CAST, expansion microscopy, locomotor activity, neuropeptide release, synaptic plasticity

1 | INTRODUCTION

Pigment-dispersing factor (PDF) is arguably the best-characterised insect “circadian” neuropeptide. PDF serves a dual signalling function by aligning the molecular clockwork of the different central clock neurons (Liang et al., 2016, 2017) and serving as a major clock output that modulates various downstream circuits (King & Sehgal, 2018; Park et al., 2000; Renn et al., 1999; Shafer & Yao, 2014). Within the *Drosophila* clock network, PDF is expressed in a small set of small and large ventrolateral neurons (sLNvs and lLNvs, respectively) that are referred to as circadian pacemaker neurons (Helfrich-Förster, 1997; Shafer & Yao, 2014). Both lLNv types as well as PDF are required for normal locomotor rhythmicity (Renn et al., 1999; Shafer & Yao, 2014). In addition to PDF, the sLNvs also express short neuropeptide F (sNPF; Johard et al., 2009) and the classic neurotransmitter glycine (Frenkel et al., 2017).

The sLNvs have dendritic processes in the accessory medulla, and terminals with mixed in- and output synapses in the superior protocerebrum (Reinhard et al., 2023). Evidence from temporal analysis of PDF immunoreactivity (Depetris-Chauvin et al., 2011; Nitabach et al., 2006; Park et al., 2000) and release of a fluorogen-activated release reporter (Klose et al., 2021) indicates that PDF release from the sLNv terminals is rhythmic and occurs during early morning. The release from terminals is dependent on membrane excitability (Depetris-Chauvin et al., 2011; Nitabach et al., 2006) and Ca^{2+} influx (Klose et al., 2021). Concomitantly, the sLNv somata show significantly higher electrical activity in the morning than in the evening (Cao et al., 2013), and intracellular free Ca^{2+} levels peak at the end of the night and decline over the day (Liang et al., 2017), though the timing of electrical activity or intracellular free Ca^{2+} changes in the soma does not directly correlate to terminal peptide release (Klose et al., 2021).

Intriguingly, the dorsal terminals of the sLNvs undergo significant time-dependent morphological changes, with maximum branching and complexity in the early morning (Zeitgeber time 2 [ZT2]) compared to early (ZT14) or late night (Fernández et al., 2008; Gorostiza et al., 2014). This time-dependent plasticity depends on temporal changes in membrane activity (Depetris-Chauvin et al., 2011; Gorostiza et al., 2014; Sivachenko et al., 2013) and is driven by the circadian clock as it persists in constant darkness (DD) but is lost in flies without a functional clock (Fernández et al., 2008). While the underlying mechanisms are not entirely clear, Fasciclin 2 (Fas2)-dependent axonal de- and re-fasciculation and Rho1-dependent axonal retraction are known to be involved (Petsakou et al., 2015; Sivachenko et al., 2013). PDF signalling is additionally required for the diel morphological plasticity, as manipulating PDF signalling or matrix metalloproteinases that degrade PDF affects the structural plasticity (Depetris-Chauvin et al., 2014).

The dorsal terminals of the sLNvs contain both presynaptic and (sparser) postsynaptic sites (Yasuyama & Meinertzhagen, 2010) and can be labelled by a dendritic marker (Petsakou et al., 2015), suggesting that they represent a mixed in- and output compartment. At least the presynaptic sites seem to undergo a daily change in numbers, in correlation with the morphological remodelling. In *Drosophila*, the presynaptic active zone is organised by Bruchpilot (BRP), a fly homolog of the vertebrate ELKS/CAST active zone proteins that clusters presynaptic Ca^{2+} channels (Fouquet et al., 2009; Ghelani & Sigrist, 2018; Kittel et al., 2006; Wagh et al., 2006). Ectopic *pdf*-Gal4-mediated expression of a tagged BRP version (BRP^{RFP}) in the sLNvs revealed a significantly higher number of BRP^{RFP}-positive puncta at circadian time 2 (CT2) compared to CT14 and CT22 (Gorostiza et al., 2014). Moreover, the number and total area of puncta labelled by a Synaptotagmin-GFP reporter (SYT^{GFP}, labels both peptidergic dense-core as well as synaptic vesicles) in *pdf*>*Syt^{sfP}* flies was increased at CT2

compared to CT14 (Gorostiza et al., 2014). Activity-dependent GFP Reconstitution Across Synaptic Partners (GRASP) further points towards a time-dependent switch of postsynaptic partners of the sLNv (Depetris-Chauvin et al., 2014). Collectively, these findings suggest that the circadian plasticity of the sLNv terminals is coupled to a change in synapse number, synaptic contacts and active zones of synaptic vesicle release. This led to a model in which the diel morphological and synaptic changes contribute to rhythmic peptidergic and transmitter output of the sLNvs which in turn drives downstream circuits regulating rhythmic behaviour and physiology. In support of this idea, overexpression of *Rho1*, which locks the terminal arborisations in a nocturnal state, leads to arrhythmic locomotor activity in constant darkness (DD; Petsakou et al., 2015), a canonical phenotype of impaired PDF signalling.

A recent study, however, genetically prevented the formation of the dorsal sLNv terminals and found that sLNv/PDF-mediated circadian output functions are unaffected (Fernandez et al., 2020). The PDF-dependent (Renn et al., 1999) bimodal diel pattern of locomotor activity as well as circadian rhythmicity and resetting of other clock cells in DD was normal in flies lacking the dorsal sLNv terminals (Fernandez et al., 2020). These findings suggest that rhythmic PDF release from the sLNvs does neither require the dorsal terminals nor their diel plasticity. Moreover, at least in isolated brains, peptides can also be released from the sLNv somata, albeit with a phase different from terminal peptide release (Klose et al., 2021). These findings raise the question to which extent PDF release requires BRP-organised presynaptic active zones in the dorsal terminals.

Here, we anatomically examined the spatial correlation between PDF-containing dense-core vesicles and release sites and BRP-organised active zones in the sLNvs at the ultrastructural level using super-resolution fluorescence and electron microscopy. We further performed a targeted RNA interference (RNAi)-based screen to test the functional relevance of sLNv-expressed structural active zone proteins and proteins of the vesicle fusion machinery for PDF signalling, using locomotor activity as a behavioural read-out. Our results suggest that PDF release from the sLNv is largely independent of the presence and localisation of BRP but requires SNARE and vesicle fusion proteins. The independence of PDF release from BRP-organised active zones helps to explain the previously reported PDF release from sLNv somata and abrogated dorsal terminals (Fernandez et al., 2020; Klose et al., 2021). Our results further suggest that BRP-labelled puncta remain stable during the day and become compacted during circadian terminal retraction at the beginning of the dark phase.

2 | MATERIAL AND METHODS

2.1 | Fly husbandry

The following genotypes of *Drosophila melanogaster* were used for synaptic labelling: UAS-brp::GFP-TR725 (BL36292; Fouquet et al., 2009), dFLEX w; *Pdf-Gal4/brp^{FOnYpet}*, UAS-FLP; +/MKRS (Gärtig et al., 2019). The lines for the targeted RNAi screen are listed in Supplementary Table 1 originated from the shRNA, KK and GD library of the Vienna *Drosophila* Resource Center (VDRC) or was a kind gift of Stephan Sigrist (Freie Universität Berlin, Germany), Paul Taghert (U Washington, St. Louis, USA) or Michael Bender (U Georgia, Athens, GA, USA).

Flies were maintained under LD 12:12 and $60 \pm 5\%$ humidity at $18 \pm 0.2^\circ\text{C}$ or $25 \pm 0.2^\circ\text{C}$ on a standard medium containing 8.0% malt extract, 8.0% corn flour, 2.2% sugar beet molasses, 1.8% yeast, 1.0% soy flour, 0.8% agar and 0.3% hydroxybenzoic acid.

2.2 | Immunocytochemistry (ICC)

Brains were dissected under a stereoscopic microscope and pooled in reaction tubes with 0.1 M phosphate-buffered saline (PBS, pH 7.4) on ice, followed by fixation in 2% paraformaldehyde and 4% sucrose in PBS for 1 hour at RT. After at least 5×5 minutes washing steps with PBS, the tissues were blocked with 5% normal goat serum (NGS) in PBS containing 0.3% Triton-X100 (PBT) for 2 hours at RT. Then, the brains were incubated in primary antibody (mouse monoclonal anti-PDF C7, 1:500–1:2000, DHSB, donated by Justin Blau; rabbit polyclonal anti-GFP 1:1000–2000, ChromoTek) solution in PBT + 5% NGS at least overnight at 4°C , followed by 6×5 minutes washes at RT with PBT. This was followed by incubation in secondary antibody (goat anti-rabbit IgG coupled to Alexa Fluor 488 or goat anti-mouse IgG coupled to Alexa Fluor 568, 1:500, Invitrogen) solution in PBT + 5% NGS for 3 hours at RT or overnight at 4°C , and washes for 4×10 minutes in PBT and 2×10 minutes in PBS at RT. The brains were then moved into a PBS droplet on a high-precision coverslip (Marienfeld, 22x22mm) with two hole-reinforcement rings (LEITZ) as a spacer. The PBS was then removed, and tissues were mounted in Vectashield 1000 (Vector Laboratories) and sealed with a second coverslip on top. Samples were stored at 4°C for a few days before scanning.

2.3 | Whole mount confocal microscopy and image analysis

Preparations were scanned on a Leica TCS SP8 confocal laser-scanning microscope (Leica Microsystems, Wetzlar, Germany) equipped with hybrid detectors, photon multiplier tubes and a white light laser for excitation, together with a 20-fold and 63-fold glycerol immersion objective (HC PL APO, Leica Microsystems, Wetzlar Germany). The acquisition parameters were set to saturation of the signal and were maintained constant throughout the scanning process. Images were processed and analysed in Fiji (Schindelin et al., 2012). To produce the figures maximum projections were compiled and brightness and contrast were linearly adjusted. The PDF signal was used to create a binary mask for each image-stack, by manually enhancing the saturation of the PDF channel before setting an arbitrary threshold to create a binary mask-stack of the neuron. The mask was used to capture the BRP signal that was co-located with PDF. Hand-defined masks were further utilised to define the compartments of the neurons: dendrites, kinks and axons. A custom-written simple Fiji macro was employed to quantify and measure the BRP particles that were included in the binary PDF mask. Mann-Whitney-U-Test in Python (SciPy-library) was used for statistical analysis.

2.4 | Quantification of PDF immunofluorescence

Flies were entrained for 5 days in LD 12:12 (100 lux at 20°C). On day 6, the animals were collected at ZT2 and ZT14 and immediately transferred to 4% paraformaldehyde in PBS, followed by fixation on a rotator for 3 hours at room temperature. After fixation, the animals were washed 3 x for 15 min with PBS. Then, the brains were dissected and blocked overnight at 4°C in NGS. The next day, the blocking solution was replaced and the brains were incubated for 48 hours at 4°C with the primary antibodies (polyclonal rabbit serum raised against cricket PDF, kind gift of Kenji Tomioka (Abdelsalam et al., 2008; 1:6000), mouse monoclonal antibody nc82 against BRP (generated by Alois Hofbauer; Wagh et al., 2006; 1:50). The brains were then rinsed five times for 10 min with PBT 0.5%, followed by incubation with secondary antibodies overnight (goat anti-rabbit IgG coupled to Alexa488, goat anti-mouse IgG coupled to Alexa647 [Jackson ImmunoResearch, Dianova, Göttingen], each 1:200). The brains were then washed 5 times for 10 min with 0.5% PBT followed by a final wash with 0.1% PBT. Afterwards, the brains were transferred to slides and aligned, then coated with mounting medium

(Vectashield 1000, Vector Laboratories) and sealed with a coverslip.

The preparations were imaged by a Leica SPE confocal microscope, using a 20x immersion objective and identical settings for all preparations. The resulting image stacks were converted to maximum projections in Fiji, and the background was subtracted. The terminal and kink regions of each hemisphere were marked as regions of interest (ROI) by the freehand tool, and integrated density and area were measured. Then, the corrected total fluorescence (CTF) was calculated as $CTF = \text{integrated density} - (\text{ROI area} * \text{mean background fluorescence})$. Differences between the genotypes were statistically assessed using a Kruskal-Wallis test followed by a Mann-Whitney U-test in OriginPro 2019 (OriginLab, Northampton MA, USA).

2.5 | Tissue expansion

For expansion microscopy (ExM, Chozinski et al., 2016), ICC was performed as described above, with a few additional steps as described earlier (Gärtig et al., 2019). After ICC, samples were transferred from the reaction tubes into a droplet of PBS on poly-Lysine coated glass slides (ThermoFisher) stabilised by a bean-shaped ring drawn with a PAP-Pen (Merck). The slides were then transferred to a moist chamber. Under the fume hood, PBS was replaced by 1 mM methacrylic-acid N-hydroxysuccinimide-ester (MA-NHS) in PBS for 1 hour at RT and then washed with PBS (3 × 5 minutes). Afterwards, tissues were incubated first in 30%, then 60% monomer solution (MS, 38% sodium acrylate, 40% acrylamide, 2% N,N'-methylenebisacrylamide, 29.2% sodium chloride, filled up by PBS to 10 ml) for 10 minutes, and then 100% MS for 30 minutes at 4°C. MS was then replaced by 80 µl of fresh 100% MS solution and a gelling chamber (coverslip with glass spacers) was placed on top. The MS solution was then removed and gelling solution (0.01% 4-hydroxy-TEMPO, 0.2% Tetram-ethylethylenediamine [TEMED] and 0.2% ammonium persulfate in MS) was added in parallel. Gelling occurred for 2–2.5 hours at 37°C.

After gelling, the chamber was carefully removed and the excess gel was cut away. To facilitate later orientation, the samples were cut into a trapezoid shape, and transferred into a six-well plate with 800 µl digestion buffer (50 mM Tris pH 8.2, containing 1 mM EDTA, 0.5% Triton X-100, 0.8 M guanidine-HCl, 8 units/ml Proteinase K, ddH₂O added to 5 ml) and digested for 2 h at 37°C. After digestion, the gels were washed with an excess volume of distilled water (5 × 10 minutes).

We also applied a post-expansion staining protocol to increase the fluorescence strength of the samples. The

protocol is similar to the standard expansion protocol above but uses a different linker and adds another staining step after the digestion and the initial expansion step. PBS was replaced by 1 mM acryloyl X-SE ester (AcX), and tissues were incubated overnight at RT and then washed with PBS (3×15 minutes). After digestion, the distilled water was replaced by PBS and the gels were incubated in primary antibody solution (5% NGS in PBS) at the same concentrations as for ICC described above at 4°C overnight. Gels were then washed with PBS (6×10 minutes) and incubated in secondary antibody solution as for ICC described above for at least 3 hours. Next, gels were washed two times with PBS and then incubated in 0.1% Hoechst 33342 for 30 min. Finally, gels were washed again with PBS (2×10 minutes) and then expanded in distilled water (5×10 minutes).

2.6 | Expansion microscopy (ExM) image analysis

After expansion and post-expansion staining, the gels were transferred onto a glass slide with a silicon spacer chamber on top. The chamber around the gel was filled with 2% low melt agarose, and sealed by a coverslip taped on top. This allowed imaging by the Leica TCS SP8 confocal laser-scanning microscope described above.

The resulting images were analysed using Fiji. First, in each optical section, regions of interest (ROIs) containing the sLNv terminals in the superior protocerebrum were defined by PDF staining, applying a soft focus and creating a binary mask. The binary mask was then used as a template to extract BRP and PDF puncta within the terminals. Next, the number and size of BRP and PDF-labelled puncta were quantified using the “analyse particles” function. As size threshold, “80 nm to infinity” was set, with an intensity threshold of 245–255 (at 8bit intensity resolution). Though we were unable to determine the exact expansion factor, we estimated an expansion of at least 2x. Given the z-resolution of 100 nm in the expanded brain, the effective z-resolution was at least in the area of around 50 nm. To analyse the distance between BRP and PDF puncta, the channels of each staining were transformed into a binary mask, using the same thresholds as described above but this time based on the individual puncta (Supplementary Figure 1). A 3D distance map was created based on the BRP mask and combined with the PDF binary mask to determine the relative distance of PDF puncta from BRP staining as grey values. The resulting distance map (Supplementary Figure 1) was processed with the PDF-mask containing the values of Euclidean distance between BRP puncta for each PDF punctum as defined by the PDF mask and

analysed with the “analyse particles” function to collect the mean value for each PDF puncta. Statistical analysis of the expansion images was performed with the Mann–Whitney-U-test in Python (scipy-library).

To quantify the density of BRP and PDF puncta in the terminals, the number of respective puncta was divided by the area of the terminal binary mask for each section of the image stack. The median of the results was calculated for each image stack and plotted.

2.7 | CATMAID

To utilize the huge dataset of the full adult female fly brain (TEMCA2) (Zheng et al., 2018), the 12 TB dataset was set up locally on an instance to enable local tracing in CATMAID (Saalfeld et al., 2009). Based on the characteristic structure of the PDF-positive sLNvs and experience from immunostained ultrastructural samples, a set of seven neurons (three respectively four on each hemisphere) was identified in the TEMCA-dataset that showed close morphological resemblance to the sLNv structure and contained dense-core vesicles. These putative s-LNvs were completely traced by hand and the ultra-structure was manually analysed for dense-core vesicle fusion events with the cell membrane in the dorsal area. The skeletons were retrieved from the local CATMAID server using the CATMAID-to-Blender Plugin (v7.0.2, Schlegel et al., 2016) for Blender (v3.5.0, blender.org). Omega fusion sites of dense-core vesicles within the putative s-LNvs were annotated by hand in CATMAID and the coordinates plotted using the rgl libraries (v1.0.1; Murdoch & Adler, 2023) in RStudio (v2022.12.0, Posit Software, PBC) for R (v4.2.2, R-project.org). The s-LNv neuron meshes from the hemibrain dataset (v1.2.1; Scheffer et al., 2020), and the automatic annotated presynaptic sites (Buhmann et al., 2021) were obtained from the neuprint server (neuprint.janelia.org) using the native libraries (v0.2.4; Bates et al., 2020) in RStudio. The neuron meshes and coordinates of the presynaptic sites were transformed to the FAFB coordinate space (FAFB14) for better comparison, using xform_brain (nat.templatebrains v1.0). The final visualisation was performed in Blender.

2.8 | Locomotor activity monitoring

Locomotor activity was monitored using commercial *Drosophila* Activity Monitors (DAM-2, Trikinetics, Waltham, USA). A 3–5 d old male flies were individually placed in small glass tubes (5 mm diameter), which contained food on one side (2% agar containing 4% sucrose) closed with

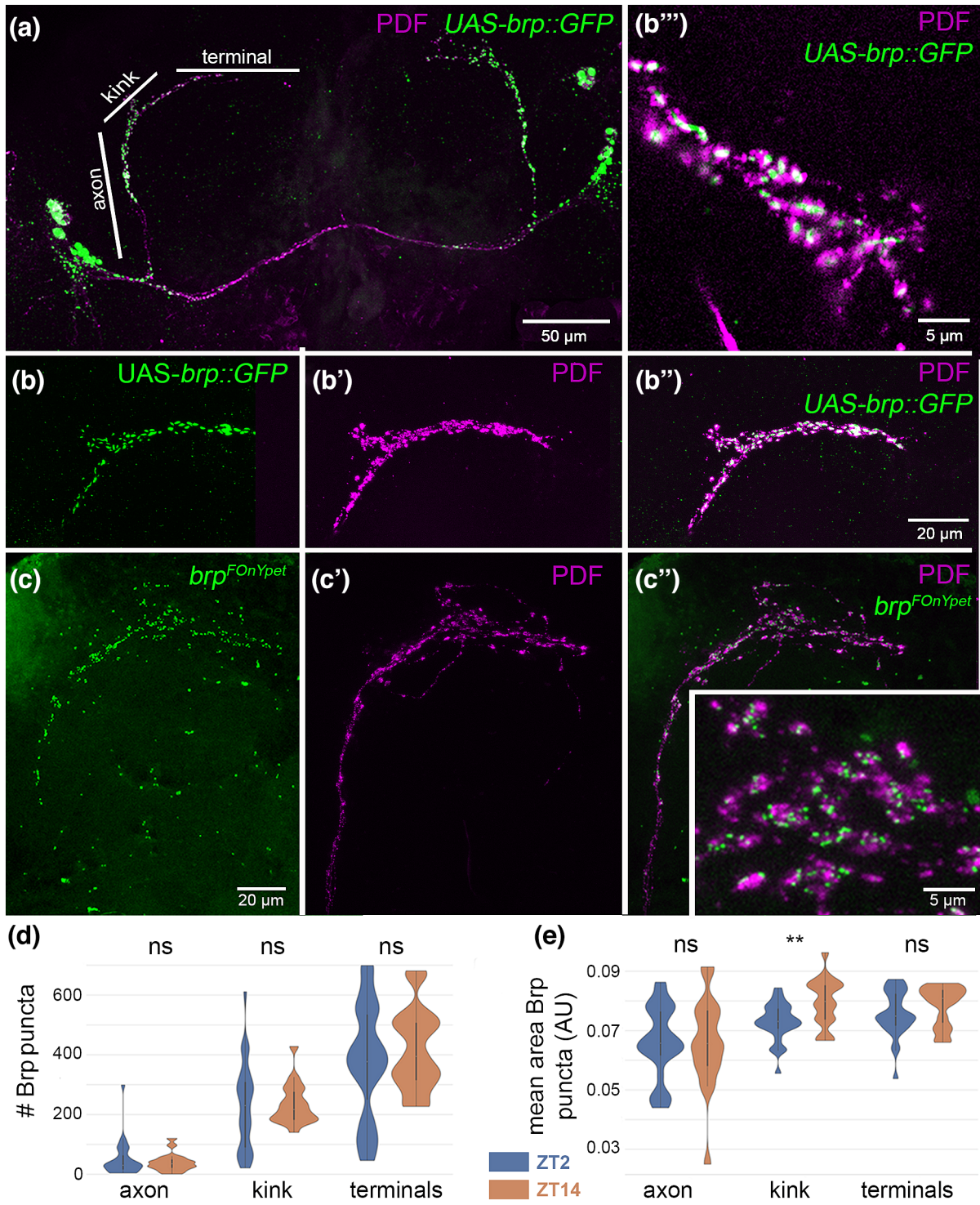


FIGURE 1 Legend on next page.

FIGURE 1 Confocal imaging of BRP^{GFP} and PDF labelling in sLNv. BRP::GFP labelling is shown in green, PDF labelling is shown in magenta. (a) Overview of the LNv morphology and Pdf-Gal4-UAS-driven expression of BRP::GFP. The sLNvs (asterisks) send lateral axons (axon) dorsally to the dorsal protocerebrum. The axon then turns from a lateral to a medial direction in the kink area to eventually arborise in the dorsal terminals in the superior protocerebrum. (b–b'') Close-up of the expression of Pdf-GAL4-UAS-driven expression of BRP::GFP (b) and PDF immunolabeling (b') in varicosities of the dorsal terminals. (b'') shows the merge of PDF and BRP^{GFP} staining. (b''') Higher magnification of the dorsal terminals in (b'') shows the accumulation of GFP::BRP in the core of the varicosities, surrounded by PDF staining that labels the sites of peptidergic dense-core vesicles. The cytoplasmic location of GFP::BRP appears to be an artefact due to overexpression by the GAL4-UAS system. (c–c'') Close-up of the expression of endogenously driven expression of BRP^{FOnYPet} (dFlex-system) (c) and PDF immunolabeling (c') in varicosities of the dorsal terminals at the same scale as (b–b''). (c'') shows the merge of PDF and BRP labelling. Insert in (c'') higher magnification (same scale as in (b''')) of the dorsal terminals shows small BRP^{FOnYPet}-labelled puncta at the membrane of the varicosities, separated from the more cytoplasmic PDF staining. (d) The number of BRP^{FOnYPet} puncta as counted by confocal microscopy was not significantly different between ZT2 and ZT14 in the axon, kink and sLNv terminals (see a). (e) The mean area of BRP^{FOnYPet} puncta was significantly higher at ZT2 than at ZT14 in the kink region, as measured by confocal microscopy. No significant change was observed between the two time points in the axon and sLNv terminals (see a).

a silicone plug. The other side was closed with a foam plug to allow for air exchange. Monitors were placed into light boxes manufactured by our workshop. The activity of the flies was measured by counting the interruptions of the infrared beam in the middle of the tubes. White light was supplied at 1 (LL) or 100 (LD) lux. Activity was monitored at a constant temperature of 20°C in LD12:12 or LD16:8 conditions for 6 days, followed by constant darkness (DD) or constant light (LL) for ten days (DD1–10 or LL1–10). Double-plotted actograms were generated by a script in R provided by Enrico Bertolini (Bertolini et al., 2019). The activity was summed into 15-minute bins. Rhythmicity parameters were analysed by autocorrelation and MESA with a MATLAB script developed by Joel Levine and colleagues (Levine et al., 2002). Flies were scored as arrhythmic if their rhythmic strength after autocorrelation was below 15. The percentage of rhythmic flies was calculated as the number of rhythmic flies divided by the total number of flies that survived for at least 10 days under constant conditions. Data distribution was tested for normality with the Shapiro–Wilk-Test and significance was calculated via the Mann–Whitney-U-Test in Python.

2.9 | Expression analysis of synaptic and vesicle release-associated proteins

Gene transcripts coding for synaptic or vesicle-release associated proteins in clock neurons (sLNvs and ILNvs) were mined in previously published single-cell RNA sequencing (scRNA-seq) datasets (Li et al., 2022; Ma et al., 2021). Pre-processing, dimensionality reduction and clustering of clock cell scRNA-seq data were performed using the original code (Ma et al., 2021). All analyses were performed with the Seurat package (v4.1.1; Hao et al., 2021) in R-Studio (v2022.02.0). Heatmaps were generated using the pheatmap package (v1.0.12).

3 | RESULTS

3.1 | Intragenic BRP markers reliably label active zones when expressed at endogenous levels

Previous work used *Pdf-GeneSwitch>UAS*-mediated ectopic expression of BRP^{RFP} to label active zones and to quantify their temporal changes (Gorostiza et al., 2014). We adopted a similar strategy by using *Pdf-Gal4* to drive full-length UAS-*brp::GFP* (Wagh et al., 2006) in the sLNvs. This construct had been used before to discriminate between dense-core vesicle release sites and active zones in the neuromuscular junction (Bulgari et al., 2019). We successfully labelled punctate structures along the whole proximal axon, the lateral flexure in the superior protocerebrum (“kink”) and the more median dorsal terminals in the superior protocerebrum (Figure 1a–b) confirming earlier findings (Gorostiza et al., 2014). Yet, the size of the BRP^{GFP}-labelled puncta was unusually large for active zones (around 1 µm at a confocal resolution; Figure 1b). Furthermore, BRP^{GFP}-labelling was not localised to the plasma membrane as expected but was localised more luminal than PDF co-immunolabelling, which indicates assemblies of peptidergic dense-core vesicles (Figure 1b). In addition, the cell bodies were strongly labelled by BRP^{GFP}. Larger dense vesicles close to BRP-containing tetrad presynaptic sites in the visual system are reported for *Drosophila* and have been suggested to carry presynaptic proteins to the active zone (Damulewicz et al., 2020). Similarly, the luminal BRP^{GFP} in our preparations may label transport vesicles that deliver BRP to active zones. However, ectopically expressed full-length BRP can aggregate (Wagh et al., 2006), and the employed *Pdf-Gal4* line is a strong peptidergic driver. Therefore, the observed unusually large size and location of BRP^{GFP} labelling in the sLNvs most likely was caused by aggregation of ectopically overexpressed BRP^{GFP}.

We therefore switched to the dFLEX system (Gärtig et al., 2019) and expressed fluorescently labelled BRP^{FOnYPet} at endogenous levels in the sLNvs. Using dFLEX, we observed labelling of membrane-associated puncta in a size range around 400 nm in confocal resolution (Figure 1c) which is compatible with the data from electron microscopic measurements at the NMJ (Kaufmann et al., 2002). We obtained similarly sized puncta after BRP^{GFP}-labelling using synaptic tagging with recombination (STaR), another method to cell-specifically label pre-synaptic proteins at endogenous levels (Chen et al., 2014) (Supplementary Figure 2). These findings suggest that endogenous labelling by fluorescent BRP constructs more reliably reports the size and distribution of active zones in the sLNv. The highest number of BRP^{FOnYPet} puncta was found in the terminals in the superior protocerebrum, followed by the region of the kink in the superior lateral protocerebrum (Figure 1d). The long proximal axonal stretch from the sLNv somata close to the accessory medulla dorsally to the kink contained much sparser BRP^{FOnYPet} labelling (Figure 1d). These results are consistent with the reported high density of synaptic input sites in the terminal and kink region, and the sparse occurrence in the proximal axonic region based on the *Janelia* hemibrain EM dataset (Shafer et al., 2022).

3.2 | The number of BRP^{FOnYPet}-labelled puncta in sLNv terminals remains stable despite circadian remodelling

The results above indicated that the dFLEX system reliably reports the size and location of BRP^{FOnYPet} active zones in the sLNvs. We next used the dFLEX system to analyse the number of BRP^{FOnYPet} puncta in different areas of PDF-immunostained sLNvs by high magnification confocal microscopy in whole-mount preparations at ZT2 and ZT14. At these times, the sLNv terminals in the dorsal protocerebrum show a high (ZT2) or low (ZT14) degree of branching (Fernández et al., 2008; Gorostiza et al., 2014). Despite the considerable daily morphological changes of the sLNv terminals, we were unable to find significant differences in the number (Mann–Whitney $p = 0.377$; Figure 1d) and mean area (Mann–Whitney $p = 0.151$; Figure 1e) of BRP^{FOnYPet} puncta in the terminal region between ZT2 ($n = 29$ images from 17 brains) and ZT14 ($n = 18$ images from 11 brains) in (Figure 1d–e) based on high-magnification confocal microscopy. Similarly, the number (Mann–Whitney $p = 0.486$; Figure 1d) and mean area (Mann–Whitney $p = 0.495$, Figure 1e) of BRP^{FOnYPet} puncta in the proximal axon region, and their number in the kink region (Mann–Whitney $p = 0.368$; Figure 1d) did not

change significantly between ZT2 and ZT14 in the same preparations (Figure 1d–e). However, we observed a significantly larger mean area in the kink region at ZT14 (Mann–Whitney, $p < 0.01$; Figure 1e).

3.3 | The density of BRP^{FOnYPet}- and PDF-labelled puncta in sLNv terminals differs between ZT2 and ZT14

The unchanged number of BRP^{FOnYPet}-labelled puncta between ZT2 and ZT14 in the sLNv is not in direct agreement with a previous study (Gorostiza et al., 2014). As the size of central synapses typically is below the resolution of confocal light microscopy, we wondered whether these results may be caused by insufficient spatial resolution and repeated the analysis with expanded brains using a previously established expansion microscopy (ExM) protocol (Gärtig et al., 2019). Unfortunately, this protocol resulted in a strong loss of staining intensity compared to the standard whole-mount protocol and would require an optimised custom-made microscopic setup to visualise BRP and PDF staining in the sLNv terminals (Figure 2a). To circumvent this issue, we performed an additional post-expansion staining which allowed us to image BRP and PDF staining in the sLNv terminals with a standard confocal microscope equipped with sensitive HyD detectors (Figure 2b–c). The subsequent quantification of the number of BRP^{FOnYPet}- and PDF-labelled puncta per area in the imaged terminal portions revealed a significant increase in the mean density of BRP^{FOnYPet}-labelled puncta (Mann–Whitney $p < 0.001$) from ZT2 to ZT14 (Figure 2d): from 3.9 ± 0.5 s.e.m. puncta/ $100 \mu\text{m}^2$ ($n = 61$ optical sections from seven brains, with each brain containing the terminals of 8 sLNvs) to 8.4 ± 0.6 s.e.m puncta/ $100 \mu\text{m}^2$ ($n = 32$ optical sections from four brains). These overall numbers are about 10x as high as reported earlier (Gorostiza et al., 2014). In part, this increase might be due to the increased spatial resolution of ExM combined with marker expression at endogenous levels. In addition, our numbers may be overestimated as we counted puncta per optical section and puncta extending between neighbouring z-sections may have been counted twice.

Furthermore, the mean density of PDF puncta increased between ZT2 to ZT14 (Figure 2c–c', e'), yet to a less pronounced extent (from 14.0 ± 0.7 s.e.m to 15.3 ± 0.9 s.e.m. per μm^2 , Mann–Whitney $p < 0.05$) than for BRP. Of note, we measured the density and not the total number of PDF puncta, and our analysis may not comprise the whole volume of terminals in the expanded brains. Thus, these results do not contradict the overall higher PDF immunofluorescence levels measured in 2D

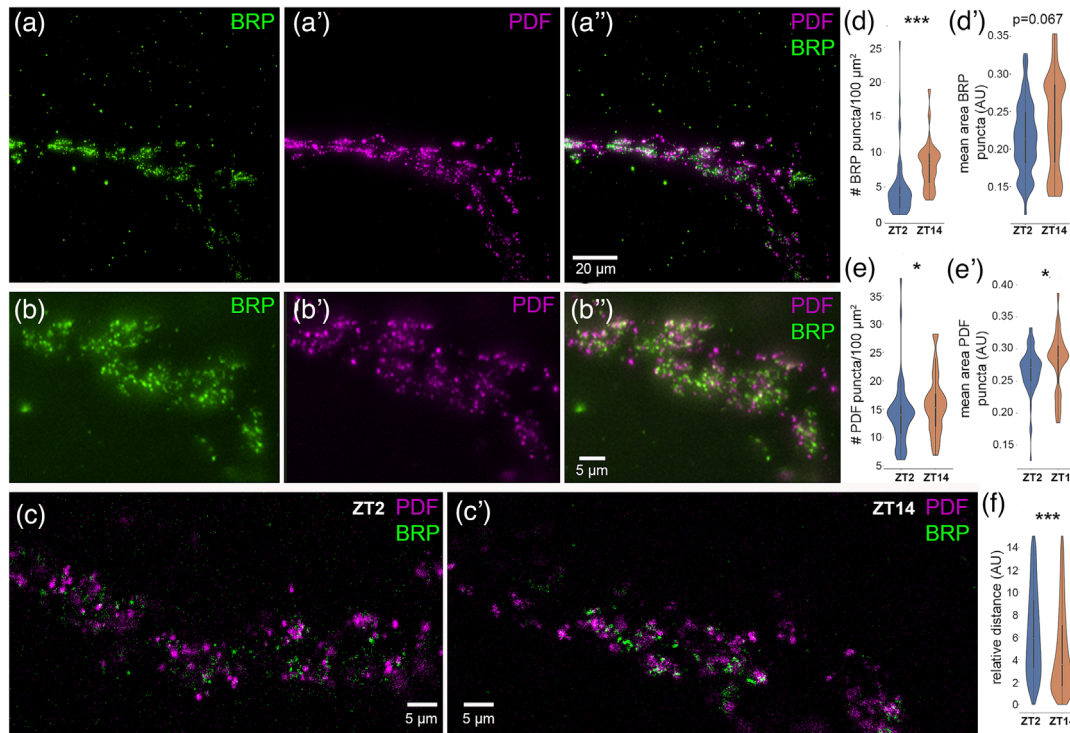


FIGURE 2 Expansion microscopy of BRP- and PDF-labelled puncta in sLNv terminals. (a–a'') distribution of BRP^{FonYPet} (a) and PDF-labelled (a') puncta in the dorsal sLNv terminals, whole stack imaged by a custom-build spinning disc confocal system (Evers lab). (b–b'') Distribution of BRP^{FonYPet} (a) and PDF-labelled (a') puncta in the dorsal sLNv terminals, whole stack imaged by a confocal laser scanning system. Independent of the confocal system, single puncta can be differentiated after expansion. (c–c') Optical section through a sLNv terminal at ZT2 (c) and ZT 14 (c'). The different puncta appear more concentrated at ZT14. (d–d') Quantification of the number (d) and relative area (d') of BRP^{FonYPet} puncta per expanded whole stack area in the terminal region suggest a strongly increased active zone density at ZT14, when the terminals are contracted, compared to ZT2 when the terminals show maximum branching. (e–e') Quantification of the number (e) and relative area (e') of PDF-labelled puncta per expanded whole stack area in the terminal region suggest a slightly increased density at ZT14, when the terminals are contracted, compared to ZT2 when the terminals show maximum branching. (f) The relative distance between BRP^{FonYPet} and PDF puncta is strongly decreased because of the increased density. Colour code: BRP^{FonYPet} (green), PDF (magenta). Scales apply to the expanded brain.

widefield or confocal maximum projections of the more branched terminals at ZT2/CT2 compared to contracted terminals at ZT/CT14 (Depetris-Chauvin et al., 2011; Nitabach et al., 2006; Park et al., 2000).

We further found that the mean area of the PDF puncta was slightly enlarged by 5% at ZT14 (Mann–Whitney $p < 0.05$, Figure 2e'). A similar trend was observed for BRP^{FonYPet} puncta (13%, Mann–Whitney $p = 0.065$, Figure 2d'). Whether this slight increase is of biological relevance or is caused by close contact between separated puncta at the time of the strongest terminal contraction remains undetermined.

In line with the increased density, the mean distance between BRP^{FonYPet} and PDF puncta was significantly reduced by 40% at ZT14 compared to ZT2 (Mann–Whitney $p < 0.001$, Figure 2f). The simplest explanation for these findings is a compaction of active zones and PDF-containing vesicles in the retracted terminals at ZT14. Unfortunately, we are unable to give precise

distances as the weak fluorescence in the expanded samples did not allow a pre-expansion scan to calculate the degree of expansion anisotropy. Collectively, our data shows that the number of BRP-organised active zones in the sLNv terminals stays fairly stable despite considerable morphological changes in the dorsal sLNv terminals between ZT2 and ZT14.

3.4 | Lack of spatial correlation between spontaneous peptidergic vesicle release and active zones

To independently test for a lack of spatial correlation between sites of dense-core vesicle release and active zones, we relied on the available dataset of an entire female adult fly brain reconstructed from serial section transmission electron microscope (ssTEM) slices (FAFB, <https://fafb.catmaid.virtualflybrain.org/>, [14609568, 0, Downloaded from <https://onlinelibrary.wiley.com/doi/10.1111/ejn.16294>, Wiley Online Library on \[24/04/2024\]. See the Terms and Conditions \(<https://onlinelibrary.wiley.com/terms-and-conditions>\) on Wiley Online Library for rules of use; OA articles are governed by the applicable Creative Commons License](https://</p>
</div>
<div data-bbox=)

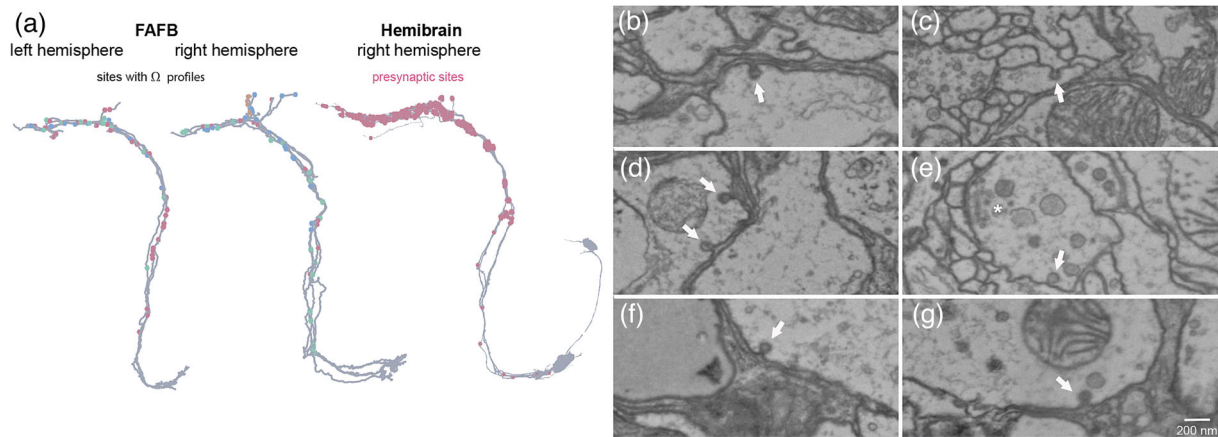


FIGURE 3 Examples of dense-core vesicle docking and fusion (Ω profiles) in the sLNv in the FAFB brain. (a) Mapping of identified membrane-docked dense-core vesicles ($n = 83$) and Ω fusion profiles ($n = 58$) to the FAFB sLNv skeletons (left), and comparison to the distribution of identified presynaptic sites in the sLNvs from the hemibrain (hemibrain data from; Shafer et al., 2022). The docked dense-core vesicles and Ω profiles are more evenly distributed in the ascending primary neurite than the presynaptic sites which are clustered to a few spots along the primary neurites. In the terminals, presynaptic sites but not docked dense-core vesicles or Ω profiles are densely clustered. Docked dense-core vesicles or Ω profiles are colour-coded according to single sLNvs (see Supplementary Figure 3). (b–g) Single TEM sections with fusing dense-core vesicles (arrows) in different anatomically identified sLNv. All Ω profiles observed were distant to active zones (also in the z-axis, not shown). (e) Shows an example where an active zone with synaptic vesicle pool (asterisks) is seen in the same section. Scale bar in (g) applies to all sections.

temca2data.org) (Zheng et al., 2018). We first identified in total seven neurons (4 in the left, 3 in the right hemisphere) that have the unique sLNv morphology and contain dense-core vesicles and reconstructed them using CATMAID (Supplementary Figure 3). We note that this morphological match does not necessarily prove the identity of these putative sLNvs in the FAFB brain. Yet, to the best of our knowledge, there is no other neuron type with similar anatomy. Further, the s-LNvs from the hemibrain (Shafer et al., 2022) transformed to the FAFB dataset fit the location and arborisation pattern of the identified neurons. In addition, the cell numbers match well (each hemisphere contains four sLNvs; Helfrich-Förster, 1997). We, therefore, concluded that these neurons are sLNvs, and went through each serial section to look for spontaneous release profiles (“ Ω profiles” formed by fusing vesicles that form an open fusion pore) of dense-core vesicles along the proximal axon, the kink and the terminal region that contains the vast majority of synaptic outputs (Shafer et al., 2022). In total, we identified 58 Ω profiles and 89 docked (non-fused vesicles at the plasma membrane) dense-core vesicles which were quite evenly distributed along the proximal axon, kink and terminal region (Figure 3a), unlike the previously described presynaptic sites of the sLNvs in the hemibrain that are clustered in the terminal and a few zones along the proximal axon (Shafer et al., 2022). None of the Ω profiles and docked dense-core vesicles were close to active zones (Figure 3b–g). While dense-core vesicles close to synaptic

vesicle pools occurred, we never observed fusion or docking of the dense-core vesicles in the immediate vicinity of these pools close to active zones. Collectively, the analysis of the FAFB ssTEM dataset supports the independence of peptidergic dense-core vesicle release from active zones and presynaptic regions of the sLNvs.

3.5 | The sLNvs express transcripts for BRP and other active zone proteins

Next, we used a bioinformatics approach to determine which genes coding for a targeted set of synaptic proteins are expressed in the sLNvs, relying on available single-cell RNAseq data of clock neurons from the Rosbash lab (Ma et al., 2021). sLNvs were identified and differentiated from the large LNvs (ILNvs) based on the co-expression of PDF, sNPF and AstC-receptor 2 (Ast-C R2), while the ILNvs express PDF but neither sNPF nor Ast-C R2 (Johard et al., 2009; Ma et al., 2021) (Figure 4a–b). We found all targeted active zone and SNARE protein genes to be expressed in both the small and large LNvs (Figure 4c), along with the gene coding for Calcium-dependent secretion activator (*Cadps*), a protein required for synaptic- and dense-core vesicle exocytosis (Renden et al., 2001). We further found expression of *amon*, a gene that encodes the prohormone convertase dPC2 required for posttranslational neuropeptide processing (Wegener et al., 2011) including PDF (Lee et al., 2023). Transcript

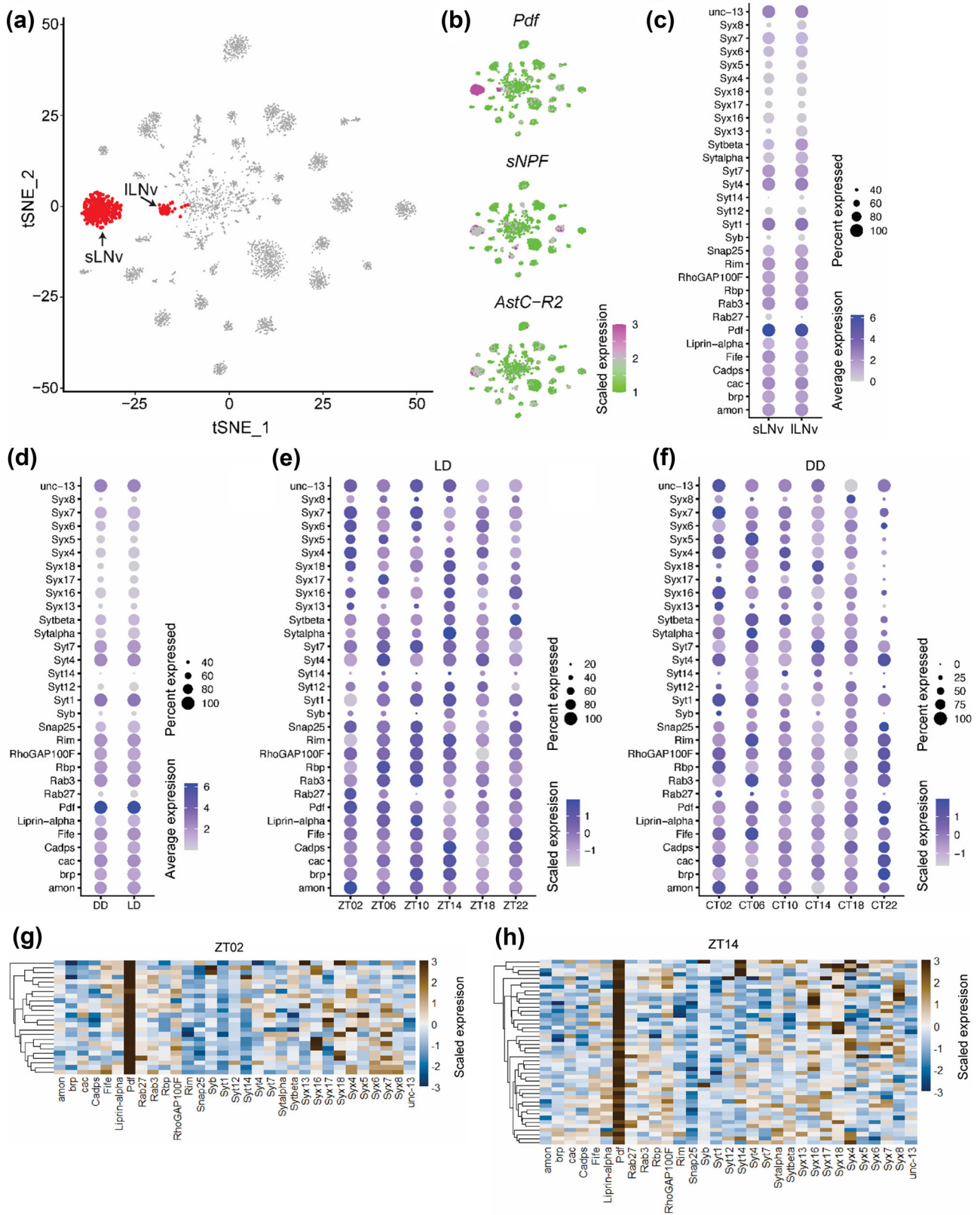


FIGURE 4 Legend on next page.

FIGURE 4 Single-cell transcriptome analysis of clock neurons. (a) A tSNE plot of clock neuron (Clk856-GAL4) single-cell transcriptomes showing large ventrolateral neuron (ILNv) and small ventrolateral neuron (sLNv) cell clusters. (b) tSNE plots showing expression of pigment dispersing factor (*Pdf*), small neuropeptide F (*sNPF*) and allatostatin-C receptor 2 (*AstC-R2*). *Pdf* is highly expressed in both ILNvs and sLNvs but *sNPF* and *AstC-R2* are expressed in sLNvs but not ILNvs. (c) Dot plot showing expression of genes in ILNvs and sLNvs. (d–f) Expression of genes under light–dark conditions (LD – 12 h light:12 h dark) and under constant darkness (DD). Data based on 329 sLNv and 70 ILNv single-cell transcriptomes. (d) Dot plot comparing expression of genes under DD and LD. (e) Dot plot comparing expression of genes at six different timepoints under LD conditions. (f) Dot plot comparing expression of genes at six different timepoints under DD conditions. (g–h) Comparison of gene expression at specific timepoints reveals sLNv heterogeneity. Heatmaps showing expression of genes at (g) ZT2 and (h) ZT14. Each row represents a single cell. *Pdf* is highly expressed in all cells, but expression of other genes is variable between different cells and across different time points. [Correction added on 11 March 2024, after first online publication: Figure 4 has been updated in this version.]

expression for the targeted synaptic proteins seems to occur independent of light input, as the expression levels were similar between LD and DD conditions (Figure 4d). While diel or circadian changes in expression levels are visible for all analysed synaptic proteins, the various transcripts are not synchronised with each other and do not cycle in phase with *Pdf* transcripts (Figure 4e–f). *Pdf* expression is highest from ZT22–ZT06/CT22–CT02. This is in line with a significantly higher number of PDF puncta at ZT2 compared to ZT14, and PDF release during the early light phase (Klose et al., 2021; Park et al., 2000) when fast Ca^{2+} activity peaks in the “morning neurons” (Liang et al., 2022). Yet, it is out of phase with *brp* expression which is highest during ZT14–18/CT14–22 (Figure 4e–f). This temporal mismatch provides additional support for a BRP-independent exocytosis of PDF.

3.6 | CADPS and SNARE proteins, but not BRP are required for PDF-dependent locomotor rhythmicity

The data above-provided evidence that PDF dense-core vesicle release is independent of BRP-organised active zones. To test whether BRP and associated active zone proteins are functionally required for PDF release, we performed a *Pdf*-Gal4-driven RNAi screen against a subset of the targeted synaptic and exocytosis-related genes found to be expressed in the sLNvs. Rhythmic locomotor activity was chosen as the behavioural read-out, taking advantage of the high level of arrhythmic locomotor activity in DD in flies with a null mutation in the *Pdf* gene (*Pdf⁰¹*, (Renn et al., 1999). *Pdf⁰¹* mutants that remain rhythmic in DD show rather weak locomotor rhythmicity with significantly shorter periods (Renn et al., 1999). *Pdf⁰¹* mutants are further unable to delay their evening activity during long photoperiods (Yoshii et al., 2009) which prompted us to use long day conditions (LD16:8). *Pdf⁰¹* mutant flies and RNAi lines against *Pdf* and *amon* were included as controls. The results are

summarised in Table 1. As expected, *Pdf⁰¹* and *Pdf*-RNAi flies became arrhythmic in DD (Figure 5a–b). In contrast, the down-regulation of *amon* did not result in a significantly altered rhythmicity, although it has been shown to be highly efficient in other peptidergic cells (Lyutova et al., 2019; Rhea et al., 2010). When expressed in the larval LNv, the employed RNAi line (*amon*-RNAi^{78b}) caused a complete lack of staining for PDF-associated peptide (a non-bioactive part of the PDF propeptide) in a third of the sampled brains, while PDF immunostaining was only significantly reduced in about a third of the samples brain, with moderate-to-strong signals in the others (Lee et al., 2023). These findings suggest that a very strong knock-down of PDF signalling is required to significantly impair locomotor rhythmicity. *Cadps*-RNAi¹¹⁰⁰⁵⁵ resulted in a strong arrhythmic phenotype, similar to complete loss or knock-down of *Pdf*. RNAi against the transcripts of the SNARE protein-coding genes *Syntaxin* (*Syx*) 1, *Syx4*, *Syx18* and neuronal *Synaptobrevin* (*nSyb*), as well as *Rbp* and *unc13A* resulted in <50% rhythmic flies and a significantly ($p < 0.01$) reduced rhythmic strength compared to *Pdf*-Gal4 controls (Figure 5a–b). *Rab3*-RNAi¹⁰⁰⁷⁸⁷ flies showed significantly reduced rhythmic strength, while 58% remained rhythmic. In contrast, none of the RNAi constructs against *brp*, *Syd-1* (*RhoGAP100F*), *liprin- α* , *RIM*, *fife*, *unc13B*, *cac*, as well as the SNARE gene *SNAP25* significantly affected rhythmicity. A loss of PDF leads to period shortening (Renn et al., 1999), which is confirmed by our results for PDF null mutants and knock-down (Table 1, Supplementary Figure 4). However, none of the lines that resulted in <50% rhythmicity showed a severely reduced period, which was only found for a combined knock-down of *Rbp* and *brp* although the single knock-downs either lengthened or had no effect on the period (Table 1, Supplementary Figure 4).

Collectively, our results suggest that vesicle-associated membrane proteins (CADPS, nSYB) and their direct cell membrane-associated partner SYX are essential parts of the machinery for PDF release. Furthermore, active zone scaffold proteins like BRP, SYD1 and LIPRIN α seem not

TABLE 1 Locomotor rhythmicity of flies with RNAi-mediated knock-down of synapse-associated proteins and controls. Period, rhythmicity and rhythmic strength (RS) derived from autocorrelation analysis. For genotypes see Supplementary Table 1.

Condition	Genotype	Period (h)	s.d.	% rhythmicity	RS	s.d.	n
DD	<i>Pdf</i> ⁰	22.6	1.9	0	4.8	3.3	25
DD	<i>PDF</i> -RNAi ⁵⁰⁷⁵⁰	23.1	1.9	3	6.2	3.7	32
DD	<i>Cadps</i> -RNAi ¹¹⁰⁰⁵⁵	24.5	1.9	3	7.5	3.3	32
DD	<i>Rbp</i> -RNAi ³⁵⁶¹⁶	24.2	1.1	38	12.7	6.7	32
DD	<i>nSyb</i> -RNAi ¹⁰⁴⁵³¹	24.5	1.0	38	13.9	5.7	32
DD	<i>Syx1A</i> -RNAi ³³¹¹²	24.3	1.0	39	13.3	9.1	32
DD	<i>Syx4</i> -RNAi ¹⁰²⁴⁶⁶	25.7	1.0	45	13.9	6.8	31
DD	<i>Syx18</i> -RNAi ¹⁰⁵¹¹³	24.0	1.5	47	13.0	9.5	32
DD	<i>unc13A</i> -RNAi ^{A1}	24.3	1.0	47	14.3	7.6	32
DD	<i>Fife</i> -RNAi ¹¹⁰⁰⁹⁹	23.8	1.0	53	16.5	6.6	32
DD	<i>Rbp</i> -RNAi, <i>brp</i> -RNAi ^{B3.C8}	23.3	0.9	55	16.1	7.2	32
DD	<i>Liprin-α</i> -RNAi ¹⁰⁶⁵⁸⁸	23.9	1.0	56	15.5	7.1	32
DD	<i>Rab3</i> -RNAi ¹⁰⁰⁷⁸⁷	24.0	0.9	58	16.1	5.9	32
DD	<i>amon</i> -RNAi ^{78b}	24.1	0.9	61	16.8	8.8	32
DD	<i>Snap25</i> -RNAi ³³⁰⁶⁴¹	23.9	1.1	62	17.3	7.3	32
DD	<i>unc13B</i> -RNAi ^{B3}	24.5	0.9	62	18	8.2	32
DD	<i>Rim</i> -RNAi ⁴⁸⁰⁷²	24.5	0.7	62	18.3	8.3	32
DD	<i>Syd1</i> -RNAi ³³⁰³⁰⁷	24.3	0.8	62	18.4	6.7	32
DD	<i>brpΔ6.1</i> ; <i>brp</i> -RNAi ^{B3.C8}	24.2	0.8	62	21.3	9.5	32
DD	<i>Cadps</i> -RNAi ²⁵²⁹²	24.3	0.7	66	19.7	7.1	32
DD	<i>Rab27</i> -RNAi ³³⁰⁷⁴⁴	24.3	0.7	67	18.8	7.3	30
DD	<i>Syd1</i> -RNAi ¹⁰⁶²⁴¹	24.1	0.7	69	17.1	5.6	32
DD	<i>Fife</i> -RNAi ¹⁰³²⁶⁷	24.7	0.8	72	19.0	6.8	32
DD	<i>Rbp</i> -RNAi	24.0	0.8	72	19.9	7.9	32
DD	<i>Pdf</i> -Gal4	24.2	0.6	72	20.3	7.2	32
DD	<i>Syt1</i> -RNAi ⁸⁸⁷⁴	24.1	0.6	74	20.1	7.3	31
DD	<i>cac</i> -RNAi ¹⁰⁴¹⁶⁸	25.0	0.6	75	20.7	6.2	32
DD	<i>Rab3</i> -RNAi ³³⁰¹⁵¹	24.3	0.7	77	18	6.3	31
DD	<i>cac</i> -RNAi ⁴⁸⁰⁹³	24.0	0.6	81	22.2	7.8	32
DD	<i>Syx1A</i> -RNAi ³³¹¹²	24.8	0.8	84	20.8	6.6	32
DD	<i>brp</i> -RNAi ^{B3.C8}	24.7	0.6	88	27.2	8.9	32
DD	<i>nSyb</i> -RNAi ⁴⁹²⁰¹	24.5	0.4	94	26.3	7.1	32
DD	<i>Rim</i> -RNAi ³⁹³⁸⁴	25.1	0.7	97	23.8	6.8	32
LL	<i>unc13B</i> -RNAi ^{B3}	24.5	2.0	3	4.8	3.9	31
LL	<i>unc13A</i> -RNAi ^{A1}	25.3	2.3	6	5.2	4.5	32
LL	<i>Rbp</i> -RNAi	24.7	1.9	12	7.15	5.4	32
LL	<i>brpΔ6.1</i> ; <i>brp</i> -RNAi ^{B3.C8}	26.4	1.6	40	10.55	10.3	32
LL	<i>Rbp</i> -RNAi; <i>brp</i> -RNAi ^{B3.C8}	25.3	1.2	58	16.4	7.4	31
LL	<i>w</i> ¹¹¹⁸ ; <i>Pdf</i> -Gal4	26.6	1.3	59	17.8	7.0	32

to be essential. A main function of BRP at the NMJ is to localize voltage-gated channels including the $\alpha 1$ subunit isoform CACOPHONY (CAC) at the active zone (Fouquet

et al., 2009); thus the lack of effect of *cac*^{RNAi} on locomotor rhythmicity provides further evidence against an important role of assembled active zones for PDF release.

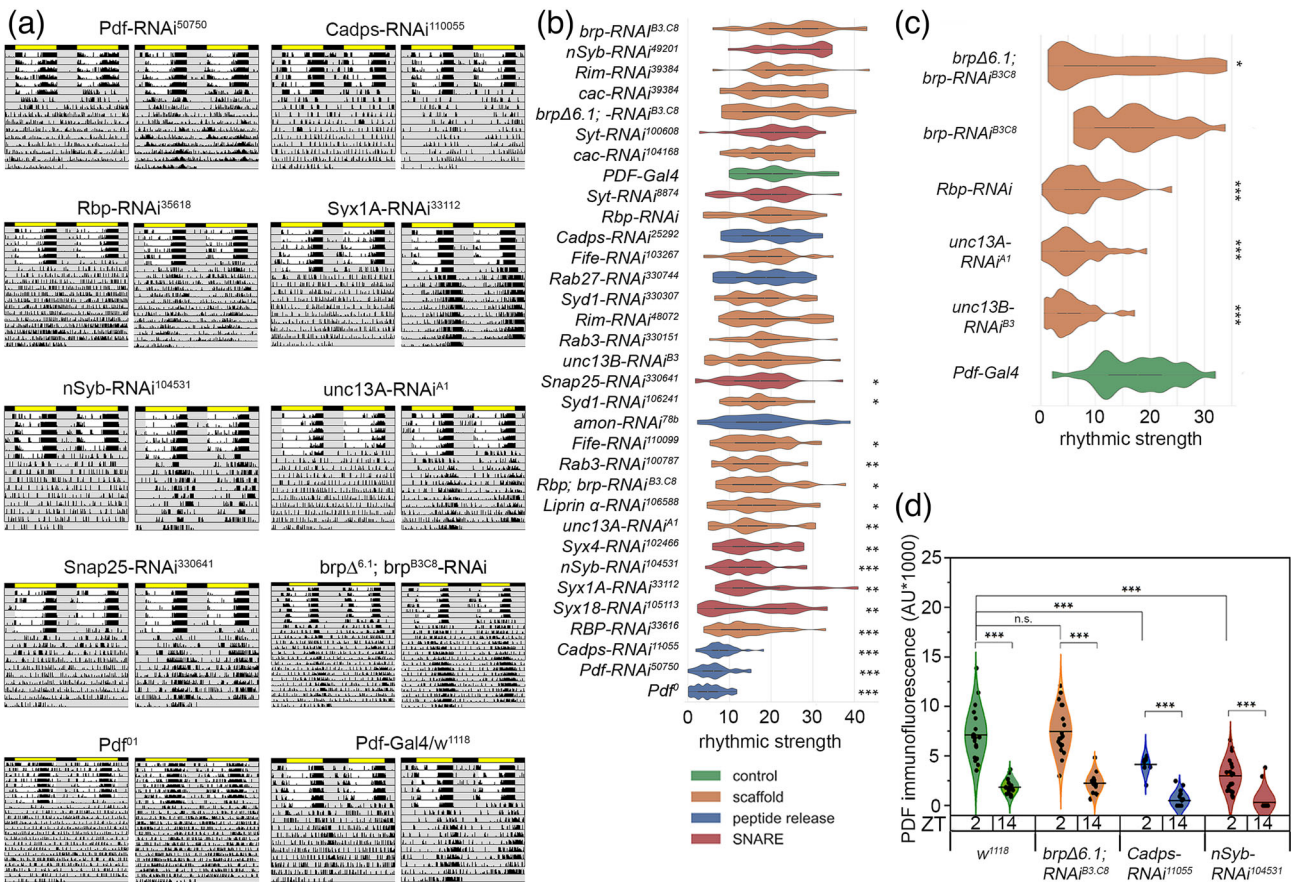


FIGURE 5 Locomotor activity, rhythmicity and PDF immunofluorescence levels after RNAi-mediated knock-down of synapse- and vesicle-release-associated genes. (a) Example actograms of individual flies after gene knock-down with the indicated RNAi lines, and in Pdf⁰¹ mutants and *w*¹¹¹⁸ controls. The left actogram shows the least rhythmic, and the right actogram the most rhythmic fly in the measured series. (b) Autocorrelation rhythmicity strength of circadian locomotor activity in DD after RNAi-mediated knockdown driven by Pdf-Gal4. The strongest reduction in rhythmicity was found for Pdf⁰¹ mutants and after the knock-down of Pdf and Cadps. A significant reduction in rhythmicity was also achieved by the knock-down of several SNARE and active zone scaffold genes, but not by various *brp* RNAi lines. (c) Autocorrelation rhythmicity strength of circadian locomotor activity in constant light (LL, 1 Lux). A strong reduction in rhythmicity after knock-down of various active zone-associated genes including *brp* is visible under these conditions uncovering glycine transmission. (d) Relative levels of PDF immunofluorescence in the sLNv terminals at ZT2 (left) and ZT14 (right) after RNAi-mediated knockdown driven by Pdf-Gal4. Each data point represents one terminal (n = 16–20) from 8 to 10 brains.

We next downregulated transcripts of core active zone scaffold proteins by RNAi in the sLNv and monitored locomotor rhythmicity under constant dim light (LL, 1 lx). Under these conditions, the majority of flies with impaired glycine signalling become arrhythmic (Frenkel et al., 2017). Glycine is a classic transmitter co-localised with PDF in the sLNvs known to be released via small synaptic vesicles at active zones. In our hands, 59% of Pdf-Gal4 controls remained rhythmic in LL, while knock-down of *unc13A*, *unc13B*, *Rbp* and *brp*^{Δ6.1}; *brp*-RNAi^{B3C8} led to a significantly lowered rhythmic strength (Figure 5c, Table 1), likely by impairing the release of glycine via small synaptic vesicles. Only *brp*-RNAi^{B3C8} had no effect, suggesting that a strong knock-down of *brp* is required to impair glycine release. The significant RNAi-

mediated downregulation of active zone scaffold protein on rhythmicity in LL suggests that the lack of effect of RNAi for BRP and other active zone scaffold proteins on PDF-dependent rhythmicity in DD is not due to inefficient transcript down-regulation. Downregulation of a putative glycine transporter is known to lengthen period (Frenkel et al., 2017). While none of the tested RNAi lines in LL resulted in increased period length compared to the *w*¹¹¹⁸; Pdf-Gal4 control, we found considerably increased period lengths in DD after down-regulation of *Syx1* and -4, *cac*, *brp* and *RIM*.

To further test the effect of RNAi against proteins involved in peptide release, we immunostained brains from three selected RNAi lines and controls against PDF at ZT2 and ZT14 in LD12:12, and quantified the

combined PDF immunofluorescent signal in the kink and terminal region (Figure 5d). In line with previous studies (Depetris-Chauvin et al., 2011; Nitabach et al., 2006; Park et al., 2000), PDF immunostaining was significantly higher at ZT2 than ZT14 in all lines tested (Figure 5d), suggesting that downregulation of *brp*, *Cadps* and *nSyb* mRNA is not affecting electrical activity (Depetris-Chauvin et al., 2011; Nitabach et al., 2006) of the sLNvs which is required for rhythmic accumulation of PDF. In addition, this finding may suggest that PDF release was not entirely blocked, even after the downregulation of *Cadps* and *nSyb*. Yet, flies with RNAi against *Cadps* and *nSyb*, but not *brpΔ6.1*; *brp*-RNAi^{B3.C8} showed strikingly reduced PDF labelling (Figure 5d). This finding correlates well with the effect strength of the RNAi lines and *Pdf⁰¹* mutants on locomotor rhythmicity (Figure 5b). Interestingly, the sLNvs express a functional PDF autoreceptor (Shafer et al., 2008) which modulates peptide release or production in an autocrine fashion (Choi et al., 2012). Overexpression of a membrane-tethered PDF construct leads to a higher resting membrane potential favouring neuronal activity, as well as increased levels of PDF immunofluorescence at ZT22 (Choi et al., 2012). Thus, the observed reduced PDF immunofluorescence may have been caused by reduced autocrine feedback due to impaired PDF release after the downregulation of *Cadps* or *nSyb*. In line, flies overexpressing *Mmp1* (a protease able to inactivate released PDF) in PDF-expressing LNvs show drastically reduced PDF immunostaining in the dorsal sLNv terminals (Depetris-Chauvin et al., 2014). Moreover, a recent study showed that the ratio between the anterograde and retrograde transport rate of vesicles in the sLNvs varies in a rhythmic fashion, resulting in an increased terminal capture of peptidergic vesicles and subsequent vesicle accumulation at the end of the night (Klose et al., 2023). This process is unlikely to be impaired after down-regulation of *Cadps* and *nSyb* and may (partially) explain the observed time-dependent changes of PDF immunofluorescent levels in *Pdf>Cadps-RNAi* and *Pdf>nSyb-RNAi* flies. Alternatively, the downregulated PDF immunofluorescence upon reduced expression of *Cadps* and *nSyb* could indicate a strongly increased release of PDF. This seems, however, less likely given that PDF expression is activity-dependent (Herrero et al., 2020) and we observed a lack-of-peptide phenotype in locomotor rhythmicity.

4 | DISCUSSION

An impressive body of knowledge exists on the terminal synaptic plasticity and circadian release of PDF from central sLNv clock neurons, as outlined in the introduction.

However, the extent to which circadian peptide release and terminal and synaptic plasticity in sLNvs are mechanistically linked to each other is ill-defined. While some researchers speculated whether rhythmic PDF levels may be a secondary consequence of circadian remodelling of the sLNv terminals (King & Sehgal, 2018) or used PDF as a marker of presynaptic boutons (Bushey et al., 2011), ultrastructural data suggested that PDF-containing dense-core vesicle are non-synaptically released (Yasuyama & Meinertzhagen, 2010).

Here we provide combined microscopic and neurogenetic evidence for an independence of PDF release from BRP-labelled active zones in the sLNvs. First, we were unable to find a spatial and numerical correlation between PDF-labelled puncta and BRP-labelled active zones using super-resolution microscopy in male brains. In addition, we found that the temporal pattern of PDF and BRP mRNA expression is not in phase with each other. Further, our RNAi screen and immunofluorescent quantification of PDF points to CADPS and a set of SNARE proteins, but not BRP or other active zone scaffold proteins as being essential for peptide release from the sLNvs in males. On the ultrastructural level, we found, based on the female FAFB brain, that the spontaneous sites of dense-core vesicle release across the sLNvs are not restricted to certain neuronal compartments and are consistently well separated from active zones, in line with earlier EM studies on sections of the sLNv terminals (Yasuyama & Meinertzhagen, 2010) or the terminal arborisations of the large PDF-expressing LNv in the visual system (Miśkiewicz et al., 2008). While sex-specific differences in the connectivity between the sLNvs may exist, it seems unlikely that there is a sex-specific mode of dense-core vesicle release. Collectively, these results suggest that PDF (and sNPF) release in the sLNv terminals is independent of BRP-organised active zones.

An unexpected finding of our study was the obvious constancy of the number of BRP puncta between the times of day with maximum (ZT2) and minimum (ZT14) branching of sLNv terminals in confocal microscopy. This should lead to an increased density of BRP puncta from ZT2 to ZT14 which was what we observed by ExM. Our data are compatible with the idea that BRP is not cyclically degraded and produced, but rather internalised and redistributed. While this clearly requires further investigation, we note that the brain-wide level of BRP isoform 190 seems to remain stable over the day (Woźnicka et al., 2015). Interestingly, a compaction of numerically unchanged BRP on a smaller mesoscale has been recently described for the *Drosophila* neuromuscular junction during presynaptic homeostatic potentiation (Dannhäuser et al., 2022; Ghelani et al., 2023; Mrestani et al., 2021). In the lamina, however, the number and size

of presynaptic profiles of the photoreceptor terminals R1-R6 and L2 monopolar cells, as well as the level of BRP are changing during BRP-dependent circadian plasticity (Górska-Andrzejak et al., 2013, 2015; Woźnicka et al., 2015). While our results do not add mechanistic insight here, it seems possible that the mechanism of circadian plasticity and the dependence on BRP differ between the sLNvs and lamina.

To functionally support the notion of a BRP-independent PDF release, we systematically downregulated transcripts of *brp* and related genes in the PDF neurons and tested whether this mimics a loss of PDF signalling. Though in general powerful, RNAi-mediated downregulation is bound to potential caveats. The RNAi downregulation may not be strong enough or have off-target effects. We therefore used at least two different RNAi constructs where possible. Second, there is a considerable degree of mutual redundancy among several active zone proteins (Ghelani & Sigrist, 2018; Held & Kaeser, 2018). To account for this, we used combinations of different RNAi constructs against BRP, performed downregulation in a heterozygous *brp* deficient background, and also performed simultaneous knockdown of *brp*- and *Rbp* that was previously developed and successfully used by the Sigrist group (Fouquet et al., 2009; Petzoldt et al., 2020; Wagh et al., 2006). In comparison to single RNAi, none of these combinations increased the effect on PDF-dependent locomotor rhythmicity in DD, but *brp* Δ 6.1; *brp*-RNAi^{B3.C8} impaired glycine-dependent locomotor activity in LL. Moreover, PDF levels appeared normal in *brp* Δ 6.1; *brp*-RNAi^{B3.C8} flies based on immunofluorescent stainings. We interpret these results as functional support for a BRP-independence of PDF release from the sLNvs. A role for ELKS in peptide release has been described for insulin secretion in pancreatic β -cells (Ohara-Imaizumi et al., 2019). Yet, peptidergic ecdysis-triggering hormone (ETH) release from the endocrine epitracheal cells also appeared to be BRP-independent (unpublished data), though BRP is expressed by those cells (Bossen et al., 2023).

The results obtained after downregulation of other active zone or vesicle release-related genes are difficult to interpret as in some cases only one of the two employed RNAi constructs gave effects. Moreover, we did not test different combinations of RNAi constructs. CADPS stands out from this, as the downregulation of its transcripts produced a strong PDF-related phenotype in locomotor activity and strongly reduced PDF immunofluorescent levels. *Cadps* RNAi was also very effective in downregulating insulin (DILP7) (Imambocus et al., 2022) and ETH signalling (unpublished data) in *Drosophila*. Thus, our results support the requirement of CADPS for dense-core vesicle release as has been previously reported

for the fly and mammals (Farina et al., 2015; Renden et al., 2001). Our results also support the role of SNARE proteins in dense-core vesicle release (Chen & Scheller, 2001; Hoogstraaten et al., 2020) and provide weak evidence for the requirement of RIM which has been shown to be essential for dense-core vesicle release in mammalian neurons (Persoon et al., 2019).

Taken together, our results based on anatomy and a functional RNAi screen infer that PDF release from the sLNvs is independent of BRP but requires CADPS and the canonical secretory vesicle fusion machinery. As BRP is a key organiser of active zones in *Drosophila* (Ghelani & Sigrist, 2018; Wagh et al., 2006), we further assume that PDF release is likely independent of BRP-organised active zones and, in principle, can occur along most axon-derived processes in a non-localised fashion. This conclusion is supported by our finding of a relatively even distribution of spontaneous peptide release events along the entire projections of the sLNvs in the FAFB brain. Moreover, a previous study showed peptide release from the soma of sLNvs (Klose et al., 2021), a compartment lacking active zones. A BRP/active zone-independent and non-localised release of PDF would also explain the mild circadian phenotype of flies with genetically abrogated sLNv terminals (Fernandez et al., 2020). From a generic perspective, active zone-independent release of peptidergic dense-core vesicles seems to be the rule rather than the exception (Bulgari et al., 2019; Ludwig & Leng, 2006; Nässel, 2009; Salio et al., 2006) and has been ultrastructurally described already more than 40 years ago across bilaterian taxa, including molluscs (Buma & Roubos, 1986), crayfish (Schürmann et al., 1991) and rats (Pow & Morris, 1988, 1989). One possibility that PDF-containing dense-core vesicles could achieve non-localised release is via the recruitment of SNARE proteins such as SYX (Gandasi & Barg, 2014; Knowles et al., 2010). This needs further testing, but we note that transcriptional down-regulation of SYX and other SNARE proteins in the LNvs significantly impaired PDF-dependent locomotor rhythmicity and, in the case of *nSyb*, led to a strong decrease in PDF immunoreactivity in this study. Our results further open the possibility that, in the sLNvs, BRP is internalised and re-localised to active zones, which theoretically would provide an efficient and cost-effective way of synaptic plasticity.

AUTHOR CONTRIBUTIONS

Conceptualization: Benedikt Hofbauer, Christian Wegener, with input from Jan Felix Evers and Meet Zandawala. **Data curation:** Benedikt Hofbauer, Nils Reinhard, Meet Zandawala. **Formal analysis:** Benedikt Hofbauer, Meet Zandawala, Nils Reinhard, Christian Wegener. **Funding acquisition:** Christian Wegener. **Investigation:** Benedikt

Hofbauer, Meet Zandawala, Jan Felix Evers, Dirk Rieger, Nils Reinhard. *Methodology*: Benedikt Hofbauer, Jan Felix Evers, Christian Werner. *Project administration*: Christian Wegener, Benedikt Hofbauer. *Resources*: Jan Felix Evers, Dirk Rieger, Christian Wegener. *Software*: Benedikt Hofbauer, Meet Zandawala, Nils Reinhard. *Supervision*: Christian Wegener, Jan Felix Evers. *Visualization*: Benedikt Hofbauer, Christian Wegener, Meet Zandawala, Nils Reinhard. *Writing—original draft*: Benedikt Hofbauer, Christian Wegener, with input from Meet Zandawala, Nils Reinhard and Dirk Rieger. *Writing—review and editing*: Meet Zandawala, Nils Reinhard, Dirk Rieger, Christian Werner, Jan Felix Evers.

ACKNOWLEDGEMENTS

We thank Markus Kiunke for setting up the server and preparing the FAFB dataset for analysis; Susanne Klühspies for technical help with immunostainings; Edwin Levitan, Stephan Sigrist and David Oswald for helpful discussions; and Michael Bender, Stephan Sigrist and Paul Taghert for the kind gift of flies. We especially thank Marta Costa and the FAFB community for creating the dataset and making it open source. Funding was provided by a programme of the Faculty of Biology, JMU (to CW) and the Deutsche Forschungsgemeinschaft (DFG, German Research Foundation: 251610680, INST 93/809-1 FUGG, for the Leica TCS SP8 microscope). Open Access funding enabled and organized by Projekt DEAL.

CONFLICT OF INTEREST STATEMENT

We declare no conflict of interests.


PEER REVIEW

The peer review history for this article is available at <https://www.webofscience.com/api/gateway/wos/peer-review/10.1111/ejn.16294>.

DATA AVAILABILITY STATEMENT


Upon publication, the data will be made publicly available at WUEDATA, the JMU research data repository, following the FAIR principles: https://wuedata.uni-wuerzburg.de/index_en.html

ORCID


Meet Zandawala  <https://orcid.org/0000-0001-6498-2208>

Nils Reinhard  <https://orcid.org/0000-0002-7989-7150>

Dirk Rieger  <https://orcid.org/0000-0001-5597-5858>

Christian Werner  <https://orcid.org/0000-0003-1281-0919>

Jan Felix Evers  <https://orcid.org/0000-0001-6377-4570>

Christian Wegener  <https://orcid.org/0000-0003-4481-3567>

REFERENCES

- Abdelsalam, S., Uemura, H., Umezaki, Y., Saifullah, A. S. M., Shimohigashi, M., & Tomioka, K. (2008). Characterization of PDF-immunoreactive neurons in the optic lobe and cerebral lobe of the cricket, *Gryllus bimaculatus*. *Journal of Insect Physiology*, *54*, 1205–1212. <https://doi.org/10.1016/j.jinsphys.2008.05.001>
- Bates, A. S., Manton, J. D., Jagannathan, S. R., Costa, M., Schlegel, P., Rohlfing, T., & Jefferis, G. S. (2020). The natverse, a versatile toolbox for combining and analysing neuroanatomical data. *eLife*, *9*, e53350. <https://doi.org/10.7554/eLife.53350>
- Bertolini, E., Schubert, F. K., Zanini, D., Sehadová, H., Helfrich-Förster, C., & Menegazzi, P. (2019). Life at high latitudes does not require circadian behavioral rhythmicity under constant darkness. *Current Biology*, *29*, 3928–3936.e3. <https://doi.org/10.1016/j.cub.2019.09.032>
- Bossen, J., Prange, R., Kühle, J.-P., Künzel, S., Niu, X., Hammel, J. U., Krieger, L., Knop, M., Ehrhardt, B., Uliczka, K., Krauss-Etschmann, S., & Roeder, T. (2023). Adult and larval tracheal systems exhibit different molecular architectures in drosophila. *International Journal of Molecular Sciences*, *24*, 5628. <https://doi.org/10.3390/ijms24065628>
- Buhmann, J., Sheridan, A., Malin-Mayor, C., Schlegel, P., Gerhard, S., Kazimiers, T., Krause, R., Nguyen, T. M., Heinrich, L., Lee, W.-C. A., Wilson, R., Saalfeld, S., Jefferis, G. S. X. E., Bock, D. D., Turaga, S. C., Cook, M., & Funke, J. (2021). Automatic detection of synaptic partners in a whole-brain Drosophila electron microscopy data set. *Nature Methods*, *18*, 771–774. <https://doi.org/10.1038/s41592-021-01183-7>
- Bulgari, D., Deitcher, D. L., Schmidt, B. F., Carpenter, M. A., Szent-Gyorgyi, C., Bruchez, M. P., & Levitan, E. S. (2019). Activity-evoked and spontaneous opening of synaptic fusion pores. *Proceedings. National Academy of Sciences. United States of America*, *116*, 17039–17044. <https://doi.org/10.1073/pnas.1905322116>
- Buma, P., & Roubos, E. W. (1986). Ultrastructural demonstration of nonsynaptic release sites in the central nervous system of the snail *lymnaea stagnalis*, the insect *periplaneta americana*, and the rat. *Neuroscience*, *17*, 867–879. [https://doi.org/10.1016/0306-4522\(86\)90051-5](https://doi.org/10.1016/0306-4522(86)90051-5)
- Bushey, D., Tononi, G., & Cirelli, C. (2011). Sleep and synaptic homeostasis: Structural evidence in drosophila. *Science*, *332*, 1576–1581. <https://doi.org/10.1126/science.1202839>
- Cao, G., Platasa, J., Pieribone, V. A., Raccuglia, D., Kunst, M., & Nitabach, M. N. (2013). Genetically targeted optical electrophysiology in intact neural circuits. *Cell*, *154*, 904–913. <https://doi.org/10.1016/j.cell.2013.07.027>
- Chen, Y., Akin, O., Nern, A., Tsui, C. Y. K., Pecot, M. Y., & Zipursky, S. L. (2014). Cell-type-specific labeling of synapses in vivo through synaptic tagging with recombination. *Neuron*, *81*, 280–293. <https://doi.org/10.1016/j.neuron.2013.12.021>
- Chen, Y. A., & Scheller, R. H. (2001). SNARE-mediated membrane fusion. *Nature Reviews. Molecular Cell Biology*, *2*, 98–106. <https://doi.org/10.1038/35052017>

- Choi, C., Cao, G., Tanenhaus, A. K., McCarthy, E. V., Jung, M., Schleyer, W., Shang, Y., Rosbash, M., Yin, J. C. P., & Nitabach, M. N. (2012). Autoreceptor control of peptide/neurotransmitter corelease from PDF neurons determines allocation of circadian activity in drosophila. *Cell Reports*, 2, 332–344. <https://doi.org/10.1016/j.celrep.2012.06.021>
- Chozinski, T. J., Halpern, A. R., Okawa, H., Kim, H.-J., Tremel, G. J., Wong, R. O. L., & Vaughan, J. C. (2016). Expansion microscopy with conventional antibodies and fluorescent proteins. *Nature Methods*, 13, 485–488. <https://doi.org/10.1038/nmeth.3833>
- Damulewicz, M., Woźnicka, O., Jasińska, M., & Pyza, E. (2020). CRY-dependent plasticity of tetrad presynaptic sites in the visual system of drosophila at the morning peak of activity and sleep. *Scientific Reports*, 10, 18161. <https://doi.org/10.1038/s41598-020-74442-w>
- Dannhäuser, S., Mrestani, A., Gundelach, F., Pauli, M., Komma, F., Kollmannsberger, P., Sauer, M., Heckmann, M., & Paul, M. M. (2022). Endogenous tagging of Unc-13 reveals nanoscale reorganization at active zones during presynaptic homeostatic potentiation. *Frontiers in Cellular Neuroscience*, 16, 1074304. <https://doi.org/10.3389/fncel.2022.1074304>
- Depetris-Chauvin, A., Berni, J., Aranovich, E. J., Muraro, N. I., Beckwith, E. J., & Ceriani, M. F. (2011). Adult-specific electrical silencing of pacemaker neurons uncouples the molecular oscillator from circadian outputs. *Current Biology*, 21, 1783–1793. <https://doi.org/10.1016/j.cub.2011.09.027>
- Depetris-Chauvin, A., Fernández-Gamba, Á., Gorostiza, E. A., Herrero, A., Castaño, E. M., & Ceriani, M. F. (2014). Mmp1 processing of the PDF neuropeptide regulates circadian structural plasticity of pacemaker neurons. *PLoS Genetics*, 10, e1004700. <https://doi.org/10.1371/journal.pgen.1004700>
- Farina, M., van de Bospoort, R., He, E., Persoon, C. M., van Weering, J. R. T., Broeke, J. H., Verhage, M., & Toonen, R. F. (2015). CAPS-1 promotes fusion competence of stationary dense-core vesicles in presynaptic terminals of mammalian neurons. *eLife*, 4, e05438. <https://doi.org/10.7554/eLife.05438>
- Fernández, M. P., Berni, J., & Ceriani, M. F. (2008). Circadian remodeling of neuronal circuits involved in rhythmic behavior. *PLoS Biology*, 6, e69. <https://doi.org/10.1371/journal.pbio.0060069>
- Fernandez, M. P., Pettibone, H. L., Bogart, J. T., Roell, C. J., Davey, C. E., Pranevicius, A., Huynh, K. V., Lennox, S. M., Kostadinov, B. S., & Shafer, O. T. (2020). Sites of circadian clock neuron plasticity mediate sensory integration and entrainment. *Current Biology*, 30, 2225–2237. <https://doi.org/10.1016/j.cub.2020.04.025>
- Fouquet, W., Oswald, D., Wichmann, C., Mertel, S., Depner, H., Dyba, M., Hallermann, S., Kittel, R. J., Eimer, S., & Sigrist, S. J. (2009). Maturation of active zone assembly by drosophila Bruchpilot. *Journal of Cell Biology*, 186, 129–145. <https://doi.org/10.1083/jcb.200812150>
- Frenkel, L., Muraro, N. I., Beltrán González, A. N., Marcora, M. S., Bernabó, G., Hermann-Luibl, C., Romero, J. I., Helfrich-Förster, C., Castaño, E. M., Marino-Busjle, C., Calvo, D. J., & Ceriani, M. F. (2017). Organization of Circadian Behavior Relies on Glycinergic transmission. *Cell Reports*, 19, 72–85. <https://doi.org/10.1016/j.celrep.2017.03.034>
- Gandasi, N. R., & Barg, S. (2014). Contact-induced clustering of syntaxin and munc18 docks secretory granules at the exocytosis site. *Nature Communications*, 5, 3914. <https://doi.org/10.1038/ncomms4914>
- Gärtig, A., Ostrovsky, A., Manhart, L., Giachello, C., Kovacevic, T., Lustig, H., Chwalla, B., Cachero, S., Baines, R. A., Landgraf, M., & Evers, J. F. (2019). Motor circuit function is stabilized during postembryonic growth by anterograde transsynaptic jelly belly - anaplastic lymphoma kinase signaling. *bioRxiv*, 841106v1. <https://doi.org/10.1101/841106>
- Ghelani, T., Escher, M., Thomas, U., Esch, K., Lützkendorf, J., Depner, H., Maglione, M., Parutto, P., Gratz, S., Matkovic-Rachid, T., Ryglewski, S., Walter, A. M., Holcman, D., O'Connor Giles, K., Heine, M., & Sigrist, S. J. (2023). Interactive nanocluster compaction of the ELKS scaffold and Cacophony Ca²⁺ channels drives sustained active zone potentiation. *Science Advances*, 9, eade7804. <https://doi.org/10.1126/sciadv.ade7804>
- Ghelani, T., & Sigrist, S. J. (2018). Coupling the structural and functional assembly of synaptic release sites. *Frontiers in Neuroanatomy*, 12, 81. <https://doi.org/10.3389/fnana.2018.00081>
- Gorostiza, E. A., Depetris-Chauvin, A., Frenkel, L., Pérez, N., & Ceriani, M. F. (2014). Circadian pacemaker neurons change synaptic contacts across the day. *Current Biology*, 24, 2161–2167. <https://doi.org/10.1016/j.cub.2014.07.063>
- Górska-Andrzejak, J., Damulewicz, M., & Pyza, E. (2015). Circadian changes in neuronal networks. *Current Opinion in Insect Science*, Insect genomics * Development and regulation, 7, 76–81. <https://doi.org/10.1016/j.cois.2015.01.005>
- Górska-Andrzejak, J., Makuch, R., Stefan, J., Görlich, A., Semik, D., & Pyza, E. (2013). Circadian expression of the presynaptic active zone protein bruchpilot in the lamina of *Drosophila melanogaster*. *Developmental Neurobiology*, 73, 14–26. <https://doi.org/10.1002/dneu.22032>
- Hao, Y., Hao, S., Andersen-Nissen, E., Mauck, W. M., Zheng, S., Butler, A., Lee, M. J., Wilk, A. J., Darby, C., Zager, M., Hoffman, P., Stoeckius, M., Papalexi, E., Mimitou, E. P., Jain, J., Srivastava, A., Stuart, T., Fleming, L. M., Yeung, B., ... Satija, R. (2021). Integrated analysis of multimodal single-cell data. *Cell*, 184, 3573–3587.e29. <https://doi.org/10.1016/j.cell.2021.04.048>
- Held, R. G., & Kaeser, P. S. (2018). ELKS active zone proteins as multitasking scaffolds for secretion. *Open Biology*, 8, 170258. <https://doi.org/10.1098/rsob.170258>
- Helfrich-Förster, C. (1997). Development of pigment-dispersing hormone-immunoreactive neurons in the nervous system of *Drosophila melanogaster*. *Journal of Comparative Neurology*, 380, 335–354. [https://doi.org/10.1002/\(SICI\)1096-9861\(19970414\)380:3<335::AID-CNE4>3.0.CO;2-3](https://doi.org/10.1002/(SICI)1096-9861(19970414)380:3<335::AID-CNE4>3.0.CO;2-3)
- Herrero, A., Yoshii, T., Ispizua, J. I., Colque, C., Veenstra, J. A., Muraro, N. I., & Ceriani, M. F. (2020). Coupling neuropeptide levels to structural plasticity in drosophila clock neurons. *Current Biology*, 30, 3154–3166.e4. <https://doi.org/10.1016/j.cub.2020.06.009>
- Hoogstraaten, R. I., van Keimpema, L., Toonen, R. F., & Verhage, M. (2020). Tetanus insensitive VAMP2 differentially restores synaptic and dense core vesicle fusion in tetanus neurotoxin treated neurons. *Scientific Reports*, 10, 10913. <https://doi.org/10.1038/s41598-020-67988-2>

- Imambocus, B. N., Zhou, F., Formozov, A., Wittich, A., Tenedini, F. M., Hu, C., Sauter, K., Macarenhas Varela, E., Herédia, F., Casimiro, A. P., Macedo, A., Schlegel, P., Yang, C.-H., Miguel-Aliaga, I., Wiegert, J. S., Pankratz, M. J., Gontijo, A. M., Cardona, A., & Soba, P. (2022). A neuropeptidergic circuit gates selective escape behavior of drosophila larvae. *Current Biology*, *32*, 149–163.e8. <https://doi.org/10.1016/j.cub.2021.10.069>
- Johard, H. A. D., Yoishii, T., Dirksen, H., Cusumano, P., Rouyer, F., Helfrich-Förster, C., & Nässel, D. R. (2009). Peptidergic clock neurons in drosophila: Ion transport peptide and short neuropeptide F in subsets of dorsal and ventral lateral neurons. *The Journal of Comparative Neurology*, *516*, 59–73. <https://doi.org/10.1002/cne.22099>
- Kaufmann, N., DeProto, J., Ranjan, R., Wan, H., & Van Vactor, D. (2002). Drosophila Liprin- α and the receptor phosphatase Dlar control synapse morphogenesis. *Neuron*, *34*, 27–38. [https://doi.org/10.1016/S0896-6273\(02\)00643-8](https://doi.org/10.1016/S0896-6273(02)00643-8)
- King, A. N., & Sehgal, A. (2018). Molecular and circuit mechanisms mediating circadian clock output in the drosophila brain. *The European Journal of Neuroscience*, *51*, 268–281. <https://doi.org/10.1111/ejn.14092>
- Kittel, R. J., Wichmann, C., Rasse, T. M., Fouquet, W., Schmidt, M., Schmid, A., Wagh, D. A., Pawlu, C., Kellner, R. R., Willig, K. I., Hell, S. W., Buchner, E., Heckmann, M., & Sigrist, S. J. (2006). Bruchpilot promotes active zone assembly, Ca²⁺ channel clustering, and vesicle release. *Science*, *312*, 1051–1054. <https://doi.org/10.1126/science.1126308>
- Klose, M. K., Bruchez, M. P., Deitcher, D. L., & Levitan, E. S. (2021). Temporally and spatially partitioned neuropeptide release from individual clock neurons. *PNAS*, *118*, e2101818118. <https://doi.org/10.1073/pnas.2101818118>
- Klose, M.K., Kim, J., & Levitan, E. (2023) Activity-dependent capture of neuropeptide vesicles prepares clock neuron synapses for daily release. *bioRxiv*. <https://doi.org/10.1101/2023.12.01.569590>
- Knowles, M. K., Barg, S., Wan, L., Midorikawa, M., Chen, X., & Almers, W. (2010). Single secretory granules of live cells recruit syntaxin-1 and synaptosomal associated protein 25 (SNAP-25) in large copy numbers. *Proceedings of the National Academy of Sciences of the United States of America*, *107*, 20810–20815. <https://doi.org/10.1073/pnas.1014840107>
- Lee, G. G., Zeng, K., Duffy, C. M., Sriharsha, Y., Yoo, S., & Park, J. H. (2023). In vivo characterization of the maturation steps of a pigment dispersing factor neuropeptide precursor in the drosophila circadian pacemaker neurons. *Genetics*, *225*, iyad118. <https://doi.org/10.1093/genetics/iyad118>
- Levine, J. D., Funes, P., Dowse, H. B., & Hall, J. C. (2002). Signal analysis of behavioral and molecular cycles. *BMC Neuroscience*, *3*, 1. <https://doi.org/10.1186/1471-2202-3-1>
- Li, H., Janssens, J., De Waegeneer, M., Kolluru, S. S., Davie, K., Gardeux, V., Saelens, W., David, F. P. A., Brbić, M., Spanier, K., Leskovec, J., McLaughlin, C. N., Xie, Q., Jones, R. C., Brueckner, K., Shim, J., Tattikota, S. G., Schnorrer, F., Rust, K., ... Aerts, S. (2022). Fly cell atlas: A single-nucleus transcriptomic atlas of the adult fruit fly. *Science*, *375*, eabk2432. <https://doi.org/10.1126/science.abk2432>
- Liang, X., Holy, T. E., & Taghert, P. H. (2016). Synchronous drosophila circadian pacemakers display nonsynchronous Ca²⁺ rhythms in vivo. *Science*, *351*, 976–981. <https://doi.org/10.1126/science.aad3997>
- Liang, X., Holy, T. E., & Taghert, P. H. (2017). A series of suppressive signals within the drosophila circadian neural circuit generates sequential daily outputs. *Neuron*, *94*, 1173–1189. <https://doi.org/10.1016/j.neuron.2017.05.007>
- Liang, X., Holy, T. E., & Taghert, P. H. (2022). Circadian pacemaker neurons display cophasic rhythms in basal calcium level and in fast calcium fluctuations. *Proceedings of the National Academy of Sciences*, *119*, e2109969119. <https://doi.org/10.1073/pnas.2109969119>
- Ludwig, M., & Leng, G. (2006). Dendritic peptide release and peptide-dependent behaviours. *Nature Reviews Neuroscience*, *7*, 126–136. <https://doi.org/10.1038/nrn1845>
- Lytova, R., Selcho, M., Pfeuffer, M., Segebarth, D., Habenstein, J., Rohwedder, A., Frantzmann, F., Wegener, C., Thum, A. S., & Pauls, D. (2019). Reward signaling in a recurrent circuit of dopaminergic neurons and peptidergic Kenyon cells. *Nature Communications*, *10*, 3097. <https://doi.org/10.1038/s41467-019-11092-1>
- Ma, D., Przybylski, D., Abruzzi, K. C., Schlichting, M., Li, Q., Long, X., & Rosbash, M. (2021). A transcriptomic taxonomy of drosophila circadian neurons around the clock. *eLife*, *10*, e63056. <https://doi.org/10.7554/eLife.63056>
- Miśkiewicz, K., Schürmann, F.-W., & Pyza, E. (2008). Circadian release of pigment-dispersing factor in the visual system of the housefly, *Musca domestica*. *The Journal of Comparative Neurology*, *509*, 422–435. <https://doi.org/10.1002/cne.21765>
- Mrestani, A., Pauli, M., Kollmannsberger, P., Repp, F., Kittel, R. J., Eilers, J., Doose, S., Sauer, M., Sirén, A.-L., Heckmann, M., & Paul, M. M. (2021). Active zone compaction correlates with presynaptic homeostatic potentiation. *Cell Reports*, *37*, 109770. <https://doi.org/10.1016/j.celrep.2021.109770>
- Murdoch, D., & Adler, D. (2023). 3D visualization using OpenGL [WWW document]. <https://dmurdoch.github.io/rgl/>
- Nässel, D. (2009). Neuropeptide signaling near and far: How localized and timed is the action of neuropeptides in brain circuits? *Invertebrate Neuroscience*, *9*, 57–75. <https://doi.org/10.1007/s10158-009-0090-1>
- Nitabach, M. N., Wu, Y., Sheeba, V., Lemon, W. C., Strumbos, J., Zelensky, P. K., White, B. H., & Holmes, T. C. (2006). Electrical hyperexcitation of lateral ventral pacemaker neurons desynchronizes downstream circadian oscillators in the fly circadian circuit and induces multiple behavioral periods. *The Journal of Neuroscience*, *26*, 479–489. <https://doi.org/10.1523/JNEUROSCI.3915-05.2006>
- Ohara-Imaizumi, M., Aoyagi, K., & Ohtsuka, T. (2019). Role of the active zone protein, ELKS, in insulin secretion from pancreatic β -cells. *Molecular Metabolism*, *27S*, S81–S91. <https://doi.org/10.1016/j.molmet.2019.06.017>
- Park, J. H., Helfrich-Förster, C., Lee, G., Liu, L., Rosbash, M., & Hall, J. C. (2000). Differential regulation of circadian pacemaker output by separate clock genes in drosophila. *Proceedings of the National Academy of Sciences USA*, *97*, 3608–3613. <https://doi.org/10.1073/pnas.97.7.3608>
- Persoon, C. M., Hoogstraaten, R. I., Nassal, J. P., van Weering, J. R. T., Kaeser, P. S., Toonen, R. F., & Verhage, M. (2019). The RAB3-RIM pathway is essential for the release of

- neuromodulators. *Neuron*, 104, 1065–1080.e12. <https://doi.org/10.1016/j.neuron.2019.09.015>
- Petsakou, A., Sapsis, T. P., & Blau, J. (2015). Circadian rhythms in Rho1 activity regulate neuronal plasticity and network hierarchy. *Cell*, 162, 823–835. <https://doi.org/10.1016/j.cell.2015.07.010>
- Petzoldt, A. G., Götz, T. W. B., Driller, J. H., Lützkendorf, J., Reddy-Alla, S., Matkovic-Rachid, T., Liu, S., Knoche, E., Mertel, S., Ugorets, V., Lehmann, M., Ramesh, N., Beuschel, C. B., Kuroopka, B., Freund, C., Stelzl, U., Loll, B., Liu, F., Wahl, M. C., & Sigrist, S. J. (2020). RIM-binding protein couples synaptic vesicle recruitment to release sites. *The Journal of Cell Biology*, 219, e201902059. <https://doi.org/10.1083/jcb.201902059>
- Pow, D. V., & Morris, J. F. (1988). Exocytosis of dense-cored vesicles from synaptic and non-synaptic release sites in the hypothalamus of the rat. *Journal of Anatomy*, 158, 214–216.
- Pow, D. V., & Morris, J. F. (1989). Dendrites of hypothalamic magnocellular neurons release neurohypophysial peptides by exocytosis. *Neuroscience*, 32, 435–439. [https://doi.org/10.1016/0306-4522\(89\)90091-2](https://doi.org/10.1016/0306-4522(89)90091-2)
- Reinhard, N., Fukuda, A., Manoli, G., Derksen, E., Saito, A., Möller, G., Sekiguchi, M., Rieger, D., Helfrich-Förster, C., Yoshii, T., & Zandawala, M. (2023). Synaptic and peptidergic connectomes of the drosophila circadian clock.
- Renden, R., Berwin, B., Davis, W., Ann, K., Chin, C.-T., Kreber, R., Ganetzky, B., Martin, T. F. J., & Broadie, K. (2001). Drosophila CAPS is an essential gene that regulates dense-Core vesicle release and synaptic vesicle fusion. *Neuron*, 31, 421–437. [https://doi.org/10.1016/S0896-6273\(01\)00382-8](https://doi.org/10.1016/S0896-6273(01)00382-8)
- Renn, S. C., Park, J. H., Rosbash, M., Hall, J. C., & Taghert, P. H. (1999). A PDF neuropeptide gene mutation and ablation of PDF neurons each cause severe abnormalities of behavioral circadian rhythms in drosophila. *Cell*, 99, 791–802. [https://doi.org/10.1016/S0092-8674\(00\)81676-1](https://doi.org/10.1016/S0092-8674(00)81676-1)
- Rhea, J. M., Wegener, C., & Bender, M. (2010). The proprotein convertase encoded by *amontillado* (*amon*) is required in drosophila corpora cardiaca endocrine cells producing the glucose regulatory hormone AKH. *PLoS Genetics*, 6, e1000967. <https://doi.org/10.1371/journal.pgen.1000967>
- Saalfeld, S., Cardona, A., Hartenstein, V., & Tomancak, P. (2009). CATMAID: Collaborative annotation toolkit for massive amounts of image data. *Bioinformatics*, 25, 1984–1986. <https://doi.org/10.1093/bioinformatics/btp266>
- Salio, C., Lossi, L., Ferrini, F., & Merighi, A. (2006). Neuropeptides as synaptic transmitters. *Cell and Tissue Research*, 326, 583–598. <https://doi.org/10.1007/s00441-006-0268-3>
- Scheffer, L. K., Xu, C. S., Januszewski, M., Lu, Z., Takemura, S., Hayworth, K. J., Huang, G. B., Shinomiya, K., Maitlin-Shepard, J., Berg, S., Clements, J., Hubbard, P. M., Katz, W. T., Umayam, L., Zhao, T., Ackerman, D., Blakely, T., Bogovic, J., Dolafi, T., ... Plaza, S. M. (2020). A connectome and analysis of the adult drosophila central brain. *eLife*, 9, e57443. <https://doi.org/10.7554/eLife.57443>
- Schindelin, J., Arganda-Carreras, I., Frise, E., Kaynig, V., Longair, M., Pietzsch, T., Preibisch, S., Rueden, C., Saalfeld, S., Schmid, B., Tinevez, J.-Y., White, D. J., Hartenstein, V., Eliceiri, K., Tomancak, P., & Cardona, A. (2012). Fiji: An open-source platform for biological-image analysis. *Nature Methods*, 9, 676–682. <https://doi.org/10.1038/nmeth.2019>
- Schlegel, P., Texada, M. J., Miroshchnikov, A., Schoofs, A., Hückesfeld, S., Peters, M., Schneider-Mizell, C. M., Lacin, H., Li, F., Fetter, R. D., Truman, J. W., Cardona, A., & Pankratz, M. J. (2016). Synaptic transmission parallels neuromodulation in a central food-intake circuit. *eLife*, 5, e16799. <https://doi.org/10.7554/eLife.16799>
- Schürmann, F.-W., Sandeman, R., & Sandeman, D. (1991). Dense-core vesicles and non-synaptic exocytosis in the central body of the crayfish brain. *Cell and Tissue Research*, 265, 493–501. <https://doi.org/10.1007/BF00340872>
- Shafer, O. T., Gutierrez, G. J., Li, K., Mildenhall, A., Spira, D., Marty, J., Lazar, A. A., & de la Paz Fernandez, M. (2022). Connectomic analysis of the drosophila lateral neuron clock cells reveals the synaptic basis of functional pacemaker classes. *eLife*, 11, e79139. <https://doi.org/10.7554/eLife.79139>
- Shafer, O. T., Kim, D. J., Dunbar-Yaffe, R., Nikolaev, V. O., Lohse, M. J., & Taghert, P. H. (2008). Widespread receptivity to neuropeptide PDF throughout the neuronal circadian clock network of drosophila revealed by real-time cyclic AMP imaging. *Neuron*, 58, 223–237. <https://doi.org/10.1016/j.neuron.2008.02.018>
- Shafer, O. T., & Yao, Z. (2014). Pigment-dispersing factor signaling and circadian rhythms in insect locomotor activity. *Current Opinion in Insect Science*, Insect genomics/Development and regulation, 1, 73–80. <https://doi.org/10.1016/j.cois.2014.05.002>
- Sivachenko, A., Li, Y., Abruzzi, K. C., & Rosbash, M. (2013). The transcription factor Mef2 links the drosophila Core clock to Fas2, neuronal morphology, and circadian behavior. *Neuron*, 79, 281–292. <https://doi.org/10.1016/j.neuron.2013.05.015>
- Wagh, D. A., Rasse, T. M., Asan, E., Hofbauer, A., Schwenkert, I., Dürrbeck, H., Buchner, S., Dabauvalle, M.-C., Schmidt, M., Qin, G., Wichmann, C., Kittel, R., Sigrist, S. J., & Buchner, E. (2006). Bruchpilot, a protein with homology to ELKS/CAST, is required for structural integrity and function of synaptic active zones in drosophila. *Neuron*, 49, 833–844. <https://doi.org/10.1016/j.neuron.2006.02.008>
- Wegener, C., Herbert, H., Kahnt, J., Bender, M., & Rhea, J. M. (2011). Deficiency of prohormone convertase dPC2 (AMONTILLADO) results in impaired production of bioactive neuropeptide hormones in drosophila. *Journal of Neurochemistry*, 118, 581–595. <https://doi.org/10.1111/j.1471-4159.2010.07130.x>
- Woźnicka, O., Görlich, A., Sigrist, S., & Pyza, E. (2015). BRP-170 and BRP190 isoforms of Bruchpilot protein differentially contribute to the frequency of synapses and synaptic circadian plasticity in the visual system of drosophila. *Frontiers in Cellular Neuroscience*, 9, 238. <https://doi.org/10.3389/fncel.2015.00238>
- Yasuyama, K., & Meinertzhagen, I. A. (2010). Synaptic connections of PDF-immunoreactive lateral neurons projecting to the dorsal protocerebrum of *Drosophila melanogaster*. *The Journal of Comparative Neurology*, 518, 292–304. <https://doi.org/10.1002/cne.22210>
- Yoshii, T., Wülbeck, C., Sehadova, H., Veleri, S., Bichler, D., Stanewsky, R., & Helfrich-Förster, C. (2009). The neuropeptide pigment-dispersing factor adjusts period and phase of

Drosophila's clock. The Journal of Neuroscience, 29, 2597–2610. <https://doi.org/10.1523/JNEUROSCI.5439-08.2009>

Zheng, Z., Lauritzen, J. S., Perlman, E., Robinson, C. G., Nichols, M., Milkie, D., Torrens, O., Price, J., Fisher, C. B., Sharifi, N., Calle-Schuler, S. A., Kmecova, L., Ali, I. J., Karsh, B., Trautman, E. T., Bogovic, J. A., Hanslovsky, P., Jefferis, G. S. X. E., Kazhdan, M., ... Bock, D. D. (2018). A complete electron microscopy volume of the brain of adult *Drosophila melanogaster*. *Cell, 174, 730–743.e22.* <https://doi.org/10.1016/j.cell.2018.06.019>

SUPPORTING INFORMATION

Additional supporting information can be found online in the Supporting Information section at the end of this article.

How to cite this article: Hofbauer, B., Zandawala, M., Reinhard, N., Rieger, D., Werner, C., Evers, J. F., & Wegener, C. (2024). The neuropeptide pigment-dispersing factor signals independently of Bruchpilot-labelled active zones in daily remodelled terminals of *Drosophila* clock neurons. *European Journal of Neuroscience, 1–21.* <https://doi.org/10.1111/ejn.16294>